The Air Quality and Health Impacts of Aviation in Asia

by

In Hwan Lee

B.S. Engineering Physics
University of California, Berkeley, 2010

SUBMITTED TO THE DEPARTMENT OF AERONAUTICS AND ASTRONAUTICS IN PARTIAL FULFILLMENT OF THE REQUIREMENTS FOR THE DEGREE OF

MASTER OF SCIENCE IN AERONAUTICS AND ASTRONAUTICS
AT THE
MASSACHUSETTS INSTITUTE OF TECHNOLOGY

SEPTEMBER 2012

Signature of Author…….....
Department of Aeronautics and Astronautics
September 2012

Certified by……..
Steven R.H. Barrett
Assistant Professor of Aeronautics and Astronautics
Thesis Supervisor

Accepted by……...…….....
Eytan H. Modiano
Professor of Aeronautics and Astronautics
Chair, Graduate Program Committee

The Air Quality and Health Impacts of Aviation in Asia

by

In Hwan Lee

Submitted to the Department of Aeronautics and Astronautics
On August 23, 2012 in Partial Fulfillment of the
Requirements for the Degree of Master of Science in
Aeronautics and Astronautics
at the Massachusetts Institute of Technology

ABSTRACT

Aviation in Asia is growing more rapidly than other regions around the world. Adverse health impacts of aviation are linked to an increase in the concentration of particulate matter smaller than 2.5 μm in diameter ($PM_{2.5}$). This thesis aims to quantify the regional-scale health impacts of aviation in Asia by modeling the air quality in Asia and applying Concentration-Response Functions (CRFs) to the aviation-attributable $PM_{2.5}$ perturbations.

In order to quantify the perturbation to the ambient air quality due to aviation emissions, the Community Multiscale Air Quality (CMAQ) model—a regional-scale chemical transport model—is utilized after its performance is evaluated in predicting ambient $PM_{2.5}$ concentrations. Aviation emissions for 2006 are from the Aviation Environmental Design Tool (AEDT), and background emissions for 2006 are generated using a combination of four Asian and global emissions inventories.

A domain average increase of approximately 15ng/m^3 in annual $PM_{2.5}$ is observed due to full flight aviation emissions, while Landing and Takeoff (LTO) cycle emissions account for an increase of approximately 0.75ng/m^3. Calculations using two different CRFs used by the EPA and the WHO estimate the following amount of aviation-attributable premature mortalities in Asia: 9400 (using the EPA CRF) or 6400 (using the WHO CRF) in the full flight scenario, and 550 or 390 in the LTO cycle scenario. Finally, comparisons to the global-scale model simulation results show consistent spatial patterns of air quality perturbations, while the regional-scale model estimates approximately 1.4 times the number of mortalities obtained from corresponding global-scale studies.

Thesis Supervisor: Steven Barrett
Title: Assistant Professor of Aeronautics and Astronautics

Acknowledgements

I would like to first thank my advisor, Professor Steven Barrett, for his support. Ever since my arrival at MIT, he has provided me with guidance and advice for my classes, research, and future career. I'm very grateful that he made himself approachable and available for his students, even with an unimaginably busy schedule. Without his help and encouraging words every week, my work at MIT wouldn't have been the same.

I also would like to sincerely appreciate the mentorship and friendship of Dr. Steve Yim. The time I got to spend with him—whether in his office during the week or on the soccer field on Sundays—was fun and helpful. From project setup to result post-processing, his advice and guidance has touched every bit of my research.

Also, I would like to thank my fellow researchers at the MIT Laboratory for Aviation and the Environment. Numerous discussions and lunch runs with Akshay, Jamin, Gideon, Fabio, Chris, Sergio, and Philip will be missed dearly. Thanks also to Dr. Robert Malina, Dr. Christoph Wollersheim, and Dr. Alex Mozdzanowska for excellent leadership.

I want to express my sincere appreciation for HongSeok Cho, my friend and brother in Christ. Without his support, I would not have been able to withstand some of the toughest times of my stay at MIT. The tears and the joy we got to share together will be remembered and treasured.

I'm extremely grateful for my family, whose overwhelming love and support for me could not be hindered even by the three-hour time zone difference. Without them, I wouldn't have been able to come this far.

Lastly and most importantly, I would like to thank God for His everlasting and overwhelming love for me. I am here today, only by His grace. Soli Deo gloria!

Contents

List of Figures

List of Tables

List of Acronyms

ACE-Asia	Asian Pacific Regional Aerosol Characterization Experiment
AEDT	Aviation Environmental Design Tool
AFE	Above Field Elevation
AGL	Above Ground Level
AMET	Atmospheric Model Evaluation Tool
AORGP	Primary Organic Aerosols
BC	Black Carbon
CB05	Carbon Bond 2005
CMAQ	Community Multiscale Air Quality
CRF	Concentration Response Function
CTM	Chemical Transport Model
EDGAR	Emissions Database for Global Atmospheric Research
EI	Emission Index
EPA	Environmental Protection Agency
FB	Fuelburn
FNL	Final operational global analysis
FSC	Fuel Sulfur Content
GBD	Global Burden of Disease
GDP	Gross Domestic Product
GEIA	Global Emissions Initiative
GEOS-Chem	Goddard Earth Observing System-Chemistry
GRUMP	Global Rural-Urban Mapping Project
HC	Hydrocarbon
INTEX-B	Intercontinental Chemical Transport Experiment-Phase B
IoA	Index of Agreement
JPROC	Photolysis rate processor for CMAQ
LTO	Landing and Take-Off
MCIP	Meteorology-Chemistry Interface Processor
NASA	National Aeronautics and Space Administration
NCEP	National Center for Environmental Protection
NMB	Normalized Mean Bias
NME	Normalized Mean Error
NMVOC	Non-Methane Volatile Organic Compound

NO_X	Oxides of nitrogen
OC	Organic Carbon
PBL	Planetary Boundary Layer
PBL	Planbureau voor de Leefomgeving (Netherlands Environmental Assessment Agency)
PEC	Primary Elemental Carbon
PM	Particulate Matter
$PM_{2.5}$	Particulate matter < 2.5 μm in diameter
PM_{10}	Particulate matter < 10 μm in diameter
PM_{FINE}	Unspecified $PM_{2.5}$
PMC	Coarse Particulate Matter
PMFO	Fuel Organics Particulate Matter
PMNV	Non-Volatile Particulate Matter
PNO_3	Primary Nitrate Aerosol
POA	Primary Organic Aerosol
PRD	Pearl River Delta
PSO_4	Primary Sulfate Aerosol
PSU/NCAR MM5	Fifth Generation Pennsylvania State University / National Center for Atmospheric Research Mesoscale Modeling
R	Correlation coefficient
RAINS-Asia	Regional Air Pollution Information and Simulation Asia
RSM	Response Surface Model
SMOKE	Sparse Matrix Operator Kernel Emissions
SO_X	Oxides of sulfur
TRACE-P	Transport and Chemical Evolution over the Pacific
T2	Temperature at 2m above ground
ULS	Ultra Low Sulfur
WHO	World Health Organization
WPS	WRF Preprocessing System
WRF	Weather Research and Forecasting
WSPD10	Wind speed at 10m above ground

1 Introduction

Aviation, with its ability to provide a rapid worldwide transportation network, is a significant contributor to the world economy. The aviation industry supported approximately 3.5% of global gross domestic product (GDP) and 56.6 million jobs worldwide in 2010 [1]. The economic impacts of aviation will likely become more significant in the future, with global aviation activity projected to grow at an average of approximately 5% per year until 2030 [2, 3, 4]. While this rapid growth in aviation activity is expected to increase the economic benefits of aviation, it will also amplify the environmental impacts of aviation. Thus, policymakers face a challenge in efforts to optimize the balance between economic benefits and environmental damages of anticipated growth in aviation activity.

1.1 The Air Quality Impacts of Aviation

Aviation can affect the environment by emitting air pollutants into the atmosphere, causing degradation of air quality. Air quality impacts of aviation can vary from local scale impacts in the vicinity of airports to regional and global scale impacts via intra- and intercontinental cruise emissions. The focus of this thesis is to analyze the regional air quality impacts of aviation in Asia.

The degradation of air quality poses a threat to human health; in particular, health impacts due to a long-term exposure to particulate matter smaller than 2.5 μm in aerodynamic diameter ($PM_{2.5}$) is found to outweigh the impacts from other species [5]. Aviation $PM_{2.5}$ that is directly emitted from an engine or formed immediately after exiting an engine is considered primary, whereas secondary particulate matter is formed through complex atmospheric chemical reactions and physical processes of emitted PM precursor species (such as NO_X, SO_X, and hydrocarbons) [6]. Both primary and secondary PM contribute to adverse air quality perturbations; thus health impacts of aviation could be quantified by taking measurements of the aviation-attributable $PM_{2.5}$ concentrations. These PM species, however, are also emitted from non-aviation anthropogenic sources, such as power generation, automobile emissions, and industrial combustion; therefore, it is a difficult to experimentally distinguish the aviation-attributable particulate matter from the

non-aviation PM, except in the locality of airports. Due to this difficulty, air quality models are generally used for impacts assessment, particularly at the regional and global scale, and policy analyses in order to attribute PM to sources.

Simultaneously occurring physical and chemical processes in the atmosphere makes it extremely complex to model the relationship between emission fluxes and ambient concentrations of air pollutants such as various $PM_{2.5}$ species. Thus, atmospheric models that can capture the effects of emission patterns, meteorology, chemical transformations, and removal processes are essential to understanding the atmospheric system as a whole [7].

The Community Multiscale Air Quality (CMAQ) and GEOS-Chem models are some of the Chemical Transport Models (CTMs) often used to model and understand the relationship between the emission patterns and the consequent effects in ambient concentrations of chemical species in the atmosphere. GEOS-Chem, a global-scale CTM, was utilized in previous studies to quantify the global air quality impacts of aviation [8, 10] with a horizontal resolution of 4° × 5°. CMAQ, on the other hand, was employed to study regional-scale air quality impacts of aviation in the United States [12, 13] and in Europe [14], with a finer horizontal resolution of 36 km and 45 km, respectively.

1.2 Motivation—Regional Air Quality Impacts of Aviation in Asia

Aviation-attributable health impacts in Asia are of growing significance for a few reasons. First, growth in aviation activity in Asia—largely led by China and India—is expected to outpace growth from all other regions in the world. China currently is the second largest market for new airplanes and the demand for air travel to, from, and within China is expected to grow at about 7.6% annually [1, 2]. India is expected to be the fourth largest market for new airplanes in the next 20 years, and is expected to experience the world's fastest annual growth rate in aviation activity at approximately 8% to 9% [2, 3].

Also led by China and India, the population in Asia is a significant fraction of the world's population. The United Nations estimates the population in Asia to be approximately 4.2 billion people—approximately 60% of the world's population—in 2011, and estimates that the

population will grow to roughly 4.5 to 5.9 billion by 2050 [15]. Because a large portion of the world's population resides in Asia, a large number of people are exposed to the increased $PM_{2.5}$ concentration due to aviation. Using simulation results of a global-scale CTM, Barrett et al. [10] estimates a global total of 10,000 premature mortalities per year due to aircraft emissions in 2006, of which roughly 35% come from India and China combined, whereas the United States accounts for approximately 5%.

For the United States, the quantified health impacts of Landing and Takeoff (LTO) emissions using a global-scale CTM (GEOS-Chem) could be compared to the results of a recent study by Ratliff et al. [12], which quantified the LTO impacts using a regional-scale CTM (CMAQ). It was found that GEOS-Chem underestimates the LTO impacts by a factor of 1.4 to 2.0 relative to the impacts quantified using CMAQ [11]. However, this factor is specific to the LTO impacts in the United States and cannot be used to estimate the regional-scale air quality impacts of aviation in other regions of the world such as Asia, calling for regional-scale air quality modeling studies in non-US regions.

In response, this thesis focuses on capturing the regional-scale air quality impacts of aviation in Asia. This study follows the recommended procedures from the US Environmental Protection Agency (EPA) [16] to apply the CMAQ model for the Asian domain, as recent studies have demonstrated that CMAQ can adequately model the regional-scale air quality in Asia [17-21]. By performing air quality impact analyses on a regional scale in the Asian domain, this thesis attempts to expand the understanding of aviation impacts at a higher resolution than the previous studies.

1.3 Thesis Outline

The rest of this thesis is organized into five chapters. Chapter 2 discusses how the regional-scale CTM (CMAQ) was set up to model air quality in the Asian domain. The performance evaluation results of this model are also presented in this chapter. Chapter 3 describes the details of background (non-aviation) anthropogenic emissions in Asia. Chapter 4 discusses the details of aviation emissions and the different aviation scenarios that were analyzed. The air quality

impacts and health impacts of aviation are discussed in Chapter 5. Then Chapter 6 concludes this thesis and discusses the limitations of this study as well as the directions of potential future work.

2 Model Setup

In order to simulate the atmosphere—a complex system that is governed by simultaneously occurring physicochemical phenomena—and its behavior, various atmospheric chemical transport models (CTMs) have been developed to simulate air quality in different spatial scales. The development of these models involves the translation of real-world processes into a set of discretized mathematical equations. However, the users of these complex models also face a challenge in setting up the appropriate CTMs for their study interests. For this thesis work, a particular regional-scale air quality model is chosen and set up in order to quantify the health impacts of aviation in Asia; this chapter presents a description of the model setup.

2.1 The CMAQ Model

The U.S. EPA's Community Multiscale Air Quality (CMAQ) model is a three-dimensional Eulerian chemical transport model, designed to meet the fundamental goal of an air quality model: "establishing the relationships among meteorology, chemical transformations, emissions of chemical species, and removal processes in the context of atmospheric pollutants" [22]. CMAQ can model the complex atmospheric system across spatial scales ranging from local to hemispheric; thus, its utilization is deemed to be suitable for studying the regional-scale air quality impacts. For the work described in this thesis, CMAQ model version 4.7.1 (CMAQ v4.7.1 [22]), the most up-to-date version of the software at the time of the research, was utilized. Within the CMAQ model, various physics and chemistry modules work together to complete the chemical transport model; for each of these modules, CMAQ provides several different numerical algorithm options. For this study, most of the modules were kept at their default settings that were recommended by the EPA with the model release [22, 23]. The details of the build parameters for this study are found in Appendix A.

In order to utilize CMAQ to model the air quality in Asia, several preparatory steps were taken before starting the simulations. First, the modeling domain needed to be defined in three spatial dimensions and in the temporal domain, in accordance with the objective and the scope of the study. Next, the inputs to the CMAQ model, such as meteorology, gridded emissions, boundary

and initial conditions were prepared for the chosen modeling domain. Lastly, the performance of the CMAQ model using the defined modeling domain and the prepared model inputs must be evaluated to ensure the credibility of the modeling platform. The remainder of this chapter explains the details of the modeling domain, model inputs, and the performance evaluation results of the setup.

2.2 Modeling Domain

The domain of interest for this study is the continent of Asia; this domain includes the top two contributors to world population in China and India, as well as many other countries with high total population or population density, such as Indonesia, Pakistan, Bangladesh, Japan, and South Korea. Figure 2-1 shows the boundaries of our modeling domain; the boundaries of the domain were placed over the ocean or countries away from the region of interest, in order to minimize the impacts of boundary conditions into the domain.

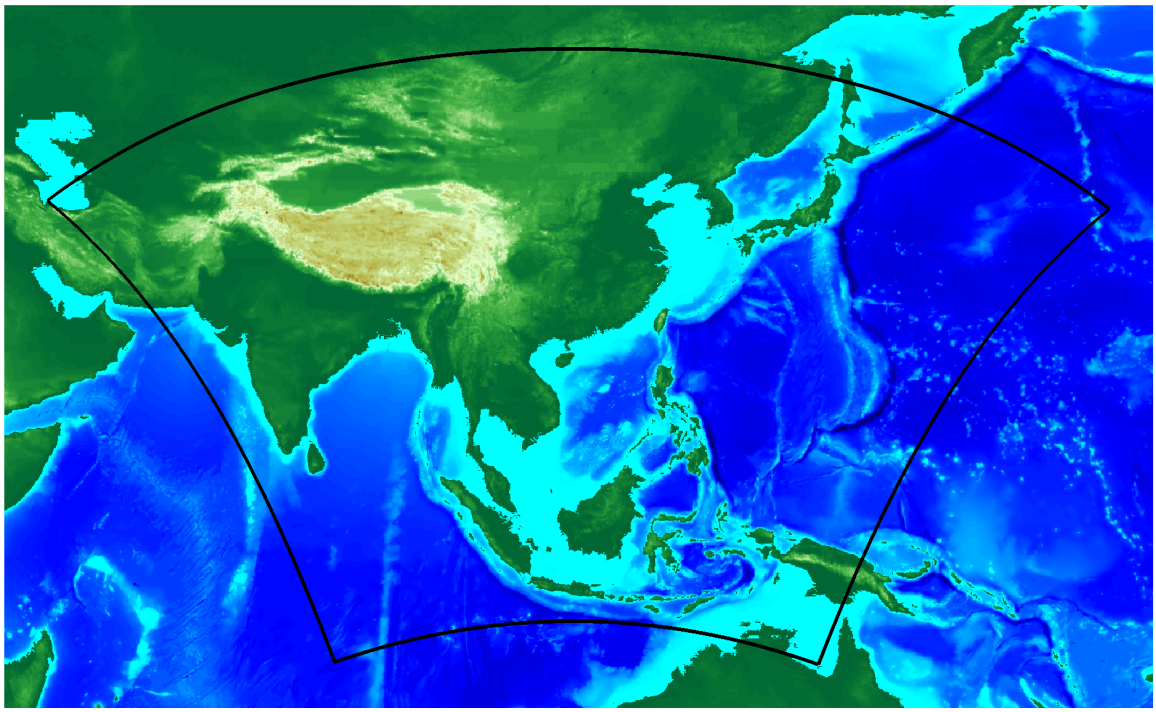

Figure 2-1: The horizontal modeling domain

Horizontally, this domain is defined by using a Lambert Conformal Conic Projection of the Earth with the projection center at (18.25°N, 110.75°E) and reference parallels at 30°N and 60°N.

There are 164 rows and 193 columns of 50km-by-50km grid cells, with the lower left corner of the domain located at 4750 km west and 4100 km south of the projection center.

The vertical domain consists of 38 terrain-following vertical layers, using a sigma coordinate system that follows Equation (2.1).

$$\sigma(p) = 1 - \frac{p - p_0}{p_{top} - p_0} \tag{2.1}$$

In this equation, p_0 is the pressure at the surface of the Earth for a given horizontal location; p_{top} is the pressure at the top of the domain, which is chosen to be 50 millibars (or approximately 20km above mean sea level) for this setup. This value of p_{top} is chosen to make sure that the model can capture the effects of aircraft emissions at cruise altitudes of 30,000 ft to 40,000 ft (or 9 km to 12 km) above ground.

Observing equation (2.1), it can be seen that the σ-values vary between $\sigma = 1$ (or $p = p_0$) at the surface of the Earth and $\sigma = 0$ (or $p = p_{top}$) at the predefined top. Considering that the health impacts are calculated using the surface-level concentration of $PM_{2.5}$, a higher accuracy (i.e. a higher resolution) in modeling the pollutant concentrations in layers near the surface is desirable. Consequently, 16 out of 38 layers are chosen to be below 1 km above ground. This tight gridding below 1km ensures that the complex vertical mixing processes within the planetary boundary layer (PBL; approximately 1km above ground [7]) is resolved.

Figure 2-2 shows the height at the top of each terrain-following vertical layer. The opaque layers indicate every 5th layer from the ground (i.e. layers 5, 10…) and the rest are transparent. It can be seen that the layers are crowded near the surface, as previously described. Also, the top layer is seen at approximately 20 km above mean sea level, and the effects of following the terrain decreases with increasing altitude.

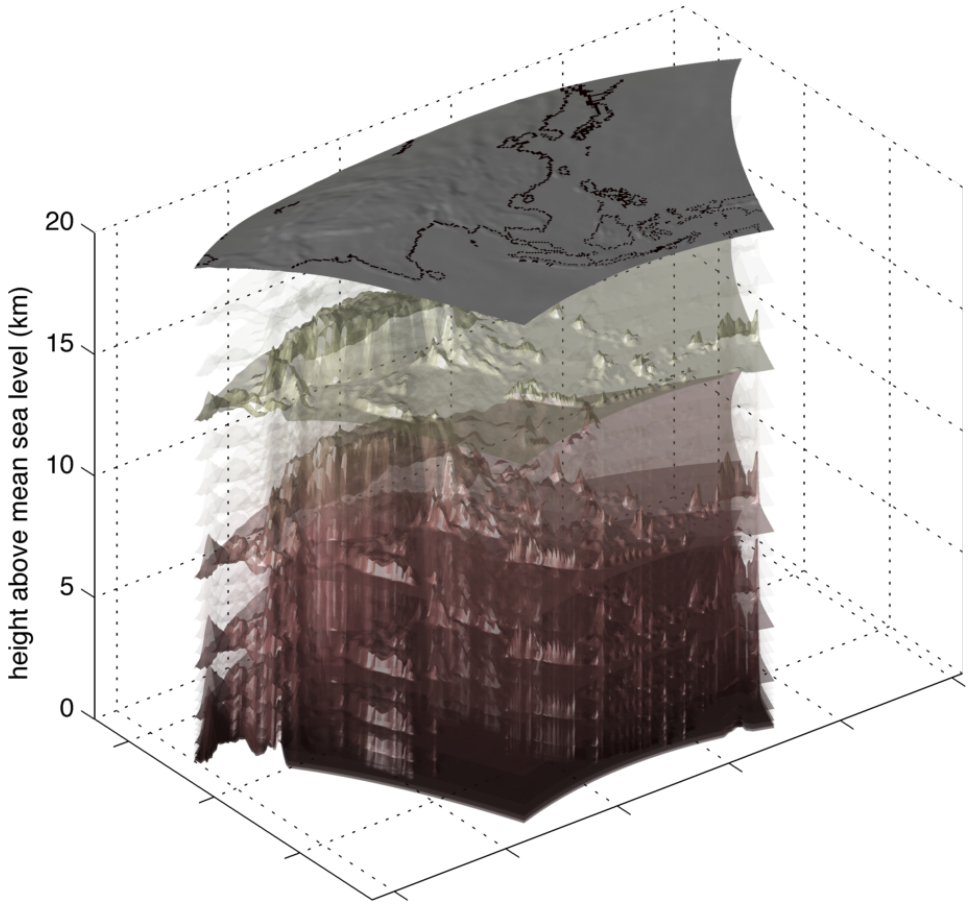

Figure 2-2: Vertical layer distribution

The temporal domain of this study is determined to be one calendar year for the following reasons. Modeling the whole calendar year captures the effects of seasonally varying meteorology that can heavily impact the pollutant concentrations; also, the temporal variation in the amount of emitted anthropogenic pollutants is taken into account. Since the health impacts are known to be associated with long-term exposure to $PM_{2.5}$, the annual mean of the pollutant concentrations are calculated. The full year CMAQ simulations are run with a spin-up period of 3 months that are disregarded; this practice is commonly used in the air quality modeling community to mitigate the effects of initial conditions by reaching a quasi-steady state at the end of the spin-up period. The duration of this spin-up is chosen to be consistent with previous modeling studies [8, 11]. A particularly long spin-up period is used for these studies to allow time for the impacts of cruise emissions to settle and be a part of the initial condition. The

modeling year for this study is 2006 due to emissions data availability; the details of the emissions data are explained in the following section, as well as Chapters 3 and 4.

2.3 Inputs to CMAQ

The goal of this thesis is to quantify the health impacts of aviation by modeling the air pollutant perturbations due to aviation. In order for the CMAQ model to be effective in quantifying the air quality impacts of aviation in Asia, it needs information about meteorology, emission patterns (both non-aviation and aviation), initial and boundary conditions of air pollutant concentrations as its inputs. These components are then used in various physics and chemistry modules in CMAQ to accurately model photochemistry, transport, and deposition of pollutants. Thus, in order for a high-fidelity model—such as CMAQ—to produce accurate modeling results, its input must be generated with the most accurate information and the most up-to-date modeling techniques. This section provides a brief description of what methods were used to generate the model inputs.

2.3.1 Meteorology

Meteorological conditions can impact air quality in various ways; it determines "the concentration levels of locally emitted primary pollutants, the formation of secondary pollutants, their transport to other areas, and their ultimate removal from the atmosphere" [7]. Therefore, in order for pollutant concentrations to be modeled for the entire modeling domain, meteorological variables such as temperature, wind, and relative humidity must be completely defined. However, measurement data from observation stations do not offer such a coverage for the entire domain; therefore, the meteorological fields themselves also need to be modeled based on the available measurement data.

Previous studies [17-21] have used the Fifth Generation Pennsylvania State University/National Center for Atmospheric Research Mesoscale Modeling (PSU/NCAR MM5), a mesoscale numerical weather prediction system designed to serve both operational forecasting and atmospheric research needs. However, with the last major release (version 3.7) in December 2004 and the last bug fix release in October 2006, NCAR decided to stop developing the MM5

model. Instead, NCAR developed Weather Research and Forecasting (WRF) model, designed to be the successor to MM5.

WRF version 3.2 [24], released in April 2010, is utilized in this study to generate meteorological fields needed for the CMAQ model. Prior to running the WRF model, the WRF Preprocessing System (WPS) is used to prepare input to the WRF model. WPS is comprised of three programs: *geogrid*, *ungrib*, and *metgrid*.

Program *geogrid* is used to define the simulation domains and to interpolate various terrestrial data to the model grids. The modeling domain for WRF simulations is set up to have five extra grids on every side, for extra buffer is needed to ensure accurate descriptions of mass flux at the boundaries of the CMAQ modeling domain [25].

Program *ungrib* processes the GRIB-formatted meteorological analysis datasets and saves them in a simpler format that can be read by *metgrid*. Analysis datasets are generated by interpolating irregularly spaced observational data from different sources to regularly spaced grids using computer-based analysis algorithms. For this study, the National Center for Environmental Protection (NCEP) Final Operational Global Analysis (FNL) dataset [26] is used. The FNL dataset is prepared on 1° by 1° horizontal grids every six hours, vertically covering the surface and 26 mandatory vertical levels. This dataset is processed last with the most complete set of observational data, compared to other analysis datasets available. This delayed generation of the FNL dataset may not be suitable for real-time applications; for this study, accuracy is more desirable over promptness, making the FNL dataset an appropriate choice. Using ungrib, the FNL dataset is processed to be the boundary and initial conditions for the WRF model.

Program *metgrid* performs horizontal interpolation of the meteorological data from the output files of *ungrib* onto the WRF domain. The outputs of *metgrid* are directly fed into the WRF model.

With the preprocessed input files for the WRF model, a 15-month simulation is performed, including the meteorological fields for the three-month CMAQ spin-up period. In order to

prevent an accumulation of computational error, WRF simulations were restarted every three modeling-days. Every restarted WRF simulation had an additional modeling-day, used as spin-up period.

The WRF model is not built specifically for air quality modeling purposes; thus, the output files from WRF simulations need to be further processed to be CMAQ-ready. This process is done using the Meteorology-Chemistry Interface Processor version 3.6 (MCIPv3.6). MCIPv3.6 takes care of the following issues: "data format translation, conversion of units of parameters, diagnostic estimations of parameters not provided, extraction of data for appropriate window domains, and reconstruction of meteorological data on different horizontal and vertical grid resolutions through interpolations as needed" [25].

The meteorological fields based on 2006 conditions are fixed across all CMAQ simulations described in this thesis. This invariability in meteorological conditions isolates the air quality impacts to changing emissions alone. Also, since meteorology is unchanging, climate-air quality feedbacks from aviation are not captured in this study.

To ensure the credibility of the WRF model, its performance must be evaluated by comparing the model results to observational data. The details of performance evaluation and the statistical parameters calculated are presented in Section 2.4.1.

2.3.2 Gridded Emissions

The amount of pollutants emitted to the atmosphere impact the pollutant concentrations both directly and indirectly. Thus, preparation of the gridded emissions input to the CMAQ model is a significant component of this thesis work. Generally, an emissions pre-processing tool is needed to translate a bulk annual emissions inventory into a CMAQ-ready gridded format. For the U.S. domain, an emissions processing software called the Sparse Matrix Operator Kernel Emissions (SMOKE) model is used to generate gridded, speciated, and hourly emissions for CMAQ, using area, biogenic, mobile, and point source emissions of various pollutant species. For the Asian region, however, no such developed tool exists. Using the framework of SMOKE, Wang et al. [28] developed SMOKE-PRD for the Pearl River Delta region; however, adapting the SMOKE

framework to the entire Asian region is still an unfinished task. Therefore, under the scope of this thesis work, tools were developed to pre-process both non-aviation ("background" from now on) and aviation emissions datasets. The details of the development of the pre-processing tool for background emissions is described in Chapter 3; the details on adapting the aviation emissions for the CMAQ modeling domain is described in Chapter 4.

The emissions species for CMAQ are determined by the choice of chemical mechanism used. For this study, the Carbon Bond 2005 (CB05) chemical mechanism [29] was selected. The CB05 mechanism contains 156 reactions involving 52 species. In accordance with the emission species that can be processed by the CB05 mechanism, the bulk annual emissions inventory is speciated into 27 different species. The list of species used in the CMAQ model for this study is listed in Appendix B.

2.3.3 Initial Conditions & Boundary Conditions

The temporal domain of this study, as described before, is 12 calendar months in 2006. However, starting the simulations with zero ambient concentrations as its initial conditions is not realistic. Therefore, a spin-up period of three months is simulated using the gridded emissions, so that the modeled atmosphere after the spin-up period would reach a quasi-steady and realistic atmospheric initial condition.

The boundary conditions for this domain are obtained from atmospheric simulation results from a global-scale CTM, GEOS-Chem [30]. Pollutant concentrations from the GEOS-Chem simulation results were interpolated onto the CMAQ modeling domain boundaries for the entire temporal domain of the simulation [31].

2.3.4 Others

CMAQ's sea-salt emissions depend on the fraction of the grid cell covered by open sea. This information is put into the CMAQ model by using an ocean file. For the U.S. domain, this ocean file can be calculated using spatial allocators. However, tools to calculate the open ocean fraction for the Asian domain is not readily available. Therefore, all the grid cells within the modeling domain are given either a value of 1 (for ocean) or 0 (for land), using the information from

geogrid output variable "landmask." Figure 2-4 shows the map of the ocean file created for the Asian domain; blue indicates the grid cells that are considered ocean and green indicates the grid cells that are considered land for the CMAQ model.

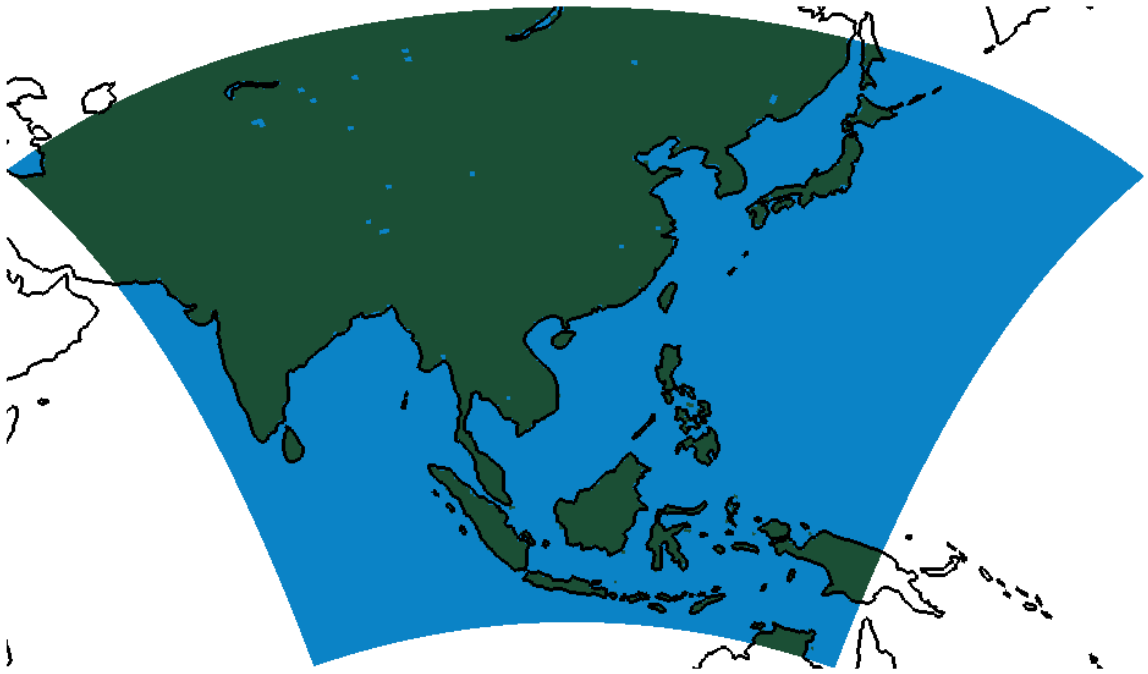

Figure 2-3: Spatial representation of the ocean file

Also, in order to model the photochemistry, information on incoming solar radiation and photolysis rates must be provided. CMAQ provides Photolysis Rate Processor (JPROC), which calculates chemical-mechanism-specific clear-sky photolysis rates that depend on altitude, solar hour angles, and latitude. JPROC calculates the photolysis rates for the CB05 chemical mechanism.

2.4 Performance Evaluation

For the impacts analysis from this study to gain its credibility, the performance of the numerical models used (both WRF for meteorology and CMAQ for air quality) must be evaluated. Both WRF and CMAQ performance evaluation validates the study year (2006) model outputs against observation data; by comparing the model outputs to the measurements, the model characteristics can be determined.

2.4.1 Statistical Parameters for Performance Evaluation

The model performance and characteristics can be quantified by using several metrics of comparison; by doing so, the metrics from this study can be compared against the same metrics obtained by other studies to determine to relative performance of the model setup.

Several statistical parameters are calculated for performance evaluations, according to the recommendations from the EPA's air quality modeling guidance [16]. Useful metrics that other studies have used for performance evaluations include the following: index of agreement (IoA), correlation coefficient (R), normalized mean error (NME), and normalized mean bias (NMB). The equations used to calculate these parameters are provided in Table 2-1.

Parameter Name	Equation
Index of Agreement (IoA)	$\text{IoA} = 1 - \frac{\sum_{i=1}^{N}(P_i - O_i)^2}{\sum_{i=1}^{N}(\lvert P_i - \overline{O}\rvert + \lvert O_i - \overline{O}\rvert)^2}$
Correlation Coefficient (R)	$R = \frac{\sum_{i=1}^{N}(P_i - \overline{P})\cdot(O_i - \overline{O})}{\sqrt{\sum_{i=1}^{N}(P_i - \overline{P})^2}\cdot\sqrt{\sum_{i=1}^{N}(O_i - \overline{O})^2}}$
Normalized Mean Error (NME)	$\text{NME} = \frac{\sum_{i=1}^{N}\lvert P_i - O_i\rvert}{\sum_{i=1}^{N} O_i}\cdot 100\%$
Normalized Mean Bias (NMB)	$\text{NMB} = \frac{\sum_{i=1}^{N}(P_i - O_i)}{\sum_{i=1}^{N} O_i}\cdot 100\%$

Table 2-1: Equations used for various statistical parameters

IoA is a parameter developed by Willmott [32] in 1981, and serves to be a standardized measure of the degree of model prediction error. The value of IoA varies between 0 and 1, where a value of 1 indicates a perfect match and a value of 0 indicates no agreement. Correlation coefficient is another metric used to quantify the strength of model prediction. The R-value varies between -1 and +1, where a value of 1 indicates a strong positive correlation and a value of -1 means a strong negative correlation. For model prediction, a value close to +1 would indicate good performance, since a perfect match between the observation and the model would mean a positive correlation.

NME is a metric used to measure the overall error of the modeling system. NME is normalized by the mean of the observation at the end, which allows a relative comparison without considering the actual magnitude of the measurements. NMB is similar to NME; the only difference is that for NMB calculation, the absolute values are not taken, allowing for a metric for quantifying the model bias.

According to the EPA [16], the recommended practice for performance evaluation of $PM_{2.5}$ is comparing the obtained results against similar modeling exercises to ensure that the model performance approximates the quality of other applications. Therefore, statistical parameters described above are compared against the same parameters obtained from previous modeling studies that focused on the regional-scale air quality modeling in Asia; the results of this comparison are presented in the subsequent sections.

2.4.2 Meteorology

For the performance evaluation of the meteorological model, the Global and U.S. Integrated Surface Hourly observation data from the National Climatic Data Center is used [33]. From this dataset, the observation data from 381 stations in China are retrieved and used. For this study, performance evaluation was conducted for the hourly values of temperature at 2m (T2) and wind speed at 10m (WSPD10).

Tables 2-2 and 2-3 show the statistical parameters for T2 and WSPD10, respectively, obtained from this study and the same parameters from Zhang et al. [18], Wang et al. [21], and Kwok et al.

[20]. Both Zhang et al. and Kwok et al. performed four 1-month simulations, for each of the four seasons of the year; therefore, in order to make a relevant comparison to this study's one-year simulation that takes into account all four seasons, the values listed on these tables are seasonal average values from the four months. Wang et al. only performed a single 1-month simulation for October 2004; although not a fair comparison, the values are listed nonetheless for completeness of comparisons to other studies.

	IoA	R	NME (%)	NMB (%)
This study (2006)	0.96	0.93	26.6	-9.4
Zhang (2008)	N/A	0.8	26.3	-12.0
Wang (10/2004)	0.97	N/A	N/A	N/A

Table 2-2: Statistical parameters obtained for temperature at 2m (T2)

	IoA	R	NME (%)	NMB (%)
This study (2006)	0.61	0.43	87.6	57.8
Zhang (2008)	N/A	0.43	81.5	58.0
Wang (10/2004)	0.79	N/A	N/A	N/A
Kwok (2004)	0.79	0.66	35.5	-2.7

Table 2-3: Statistical parameters obtained for wind speed at 10m (WSPD10)

Observing the results from Table 2-2, it is shown that this study's performance is on par with, or better than other studies' prediction of T2. However, for WSPD10, this study performs on par with Zhang et al., but significantly worse compared to Wang et al. and Kwok et al. This difference in performance may be attributed to the two studies' use of locally-available fine-resolution surface wind data used for "grid-nudging," which matches the model output to be closer to observational data provided for the nudging process.

For a graphic representation of relative performance, a "soccer goal plot" is generated. Soccer goal plots are used in the Atmospheric Model Evaluation Tool (AMET) [34]—software designed to assist in the analysis and evaluation of meteorological and air quality models—to illustrate model performance in terms of normalized mean bias (NMB) and normalized mean error (NME).

As seen in Figure 2-5, this plot presents NMB on its x-axis and NME on its y-axis; a point far away from the origin represents large values of NMB and/or NME. Points on the right-side of the y-axis represents models with positive bias; this means that model prediction is generally greater in magnitude compared to the observations.

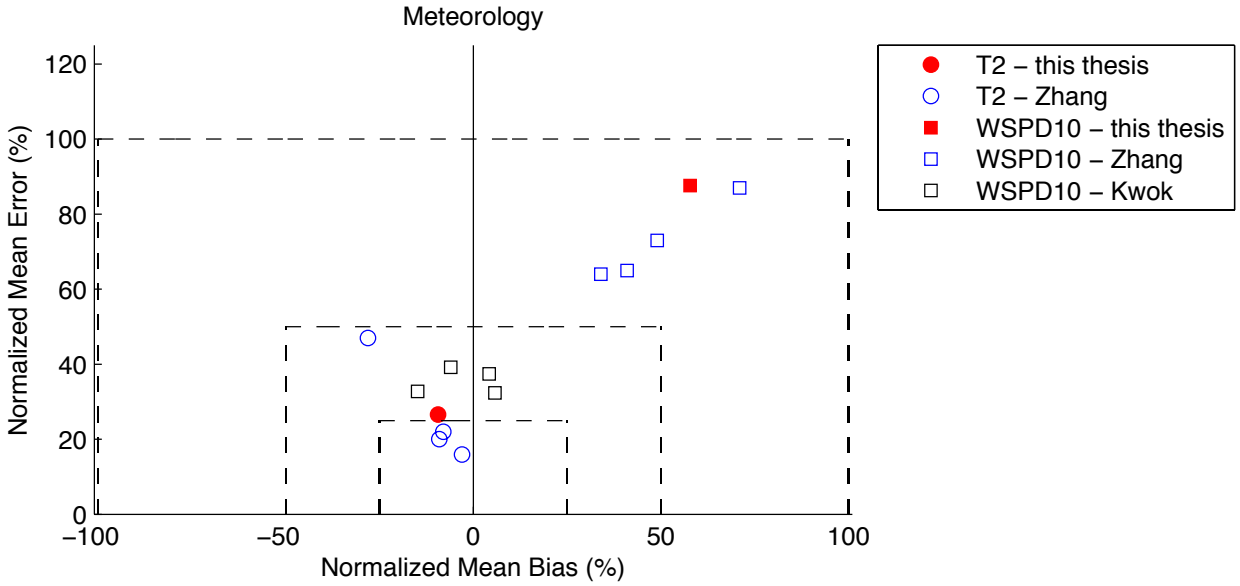

Figure 2-4: Soccer goal plot of meteorology model performance evaluation

The NMB and NME values from Table 2-2 and 2-3 are plotted in Figure 2-4. Again, this figure illustrates that this model's performance is comparative to other studies' for T2, as the circular markers are concentrated near the top edge of the 25%-soccer goal. However, the fact that they lie on the left side of the y-axis illustrates that the models generally underpredict T2. For WSPD10, there are two clusters of rectangular markers. One cluster lies near the y-axis, at about 40% NME; another cluster lies around 75% NMB and NME. The first cluster represents the studies that did not use grid-nudging, and the second cluster represents studies with grid-nudging that resulted in a better performance.

From the performance evaluation of meteorology, it is noticeable that there's a large overprediction of wind speed throughout the modeling domain. This overprediction in wind speed is likely to affect CTM performance. The next section looks at the performance evaluation of air quality.

2.4.3 Air Quality

For the performance evaluation of the air quality model, hourly observation data from three different datasets all over Asia are used [56, 94, 95]. From these datasets, hourly observation data from 66 stations are used to compare the modeled and observed concentrations of O_3, $PM_{2.5}$ and PM_{10}. Following the steps of meteorology performance evaluation, the air quality model performance evaluation results of this thesis are compared to those of other studies.

In addition to Kwok et al. [20] and Wang et al. [21], the results of Liu et al. [17] are used for comparison. Similar to other studies, Liu et al. performs four 1-month simulations to account for the seasonal variations. Tables 2-4, 2-5, and 2-6 display the statistical parameters obtained from this thesis, and the same parameters from similar scale studies used for comparison.

	IoA	R	NME (%)	NMB (%)
This study (2006)	0.68	0.56	53.20	4.12
Kwok (2004)	0.64	N/A	76.33	45.68
Liu (2008)	N/A	0.58	22.13	8.50
Wang (10/2004)	N/A	0.73	37.10	-5.40

Table 2-4: Statistical parameters obtained for O_3 concentration at ground

	IoA	R	NME (%)	NMB (%)
This study (2006)	0.42	0.16	84.20	-13.41
Kwok (2004)	0.53	N/A	52.15	-42.73

Table 2-5: Statistical parameters obtained for $PM_{2.5}$ concentration at ground

	IoA	R	NME (%)	NMB (%)
This study (2006)	0.43	0.14	70.69	-44.92
Kwok (2004)	0.51	N/A	50.30	-41.00
Liu (2008)	N/A	0.30	54.38	-43.15

Table 2-6: Statistical parameters obtained for PM_{10} concentration at ground

The same statistical parameters are also displayed, using a soccer goal plot, in Figure 2-5, in order to visualize the comparison between this thesis work and other studies.

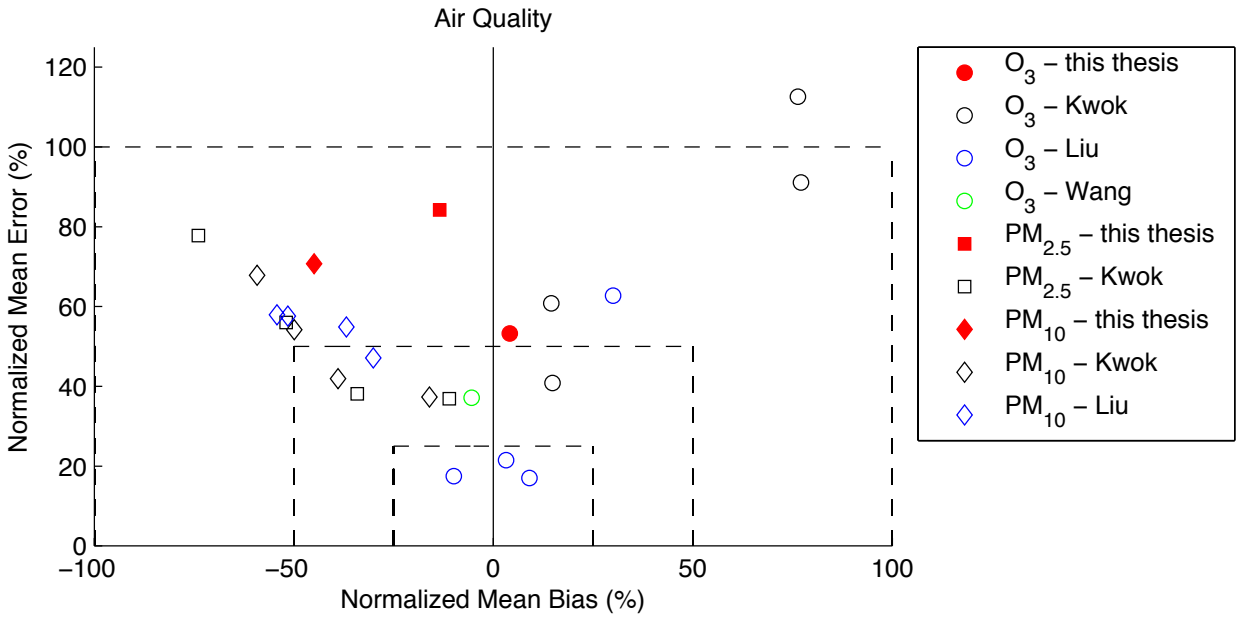

Figure 2-5: Soccer goal of air quality model performance evaluation

From observing Tables 2-4 to 2-6 and Figure 2-5, this model's performance is comparative to other studies' for O_3 concentration; however, its performance for PM species is not as competitive. This pattern can be attributed to the relative performance of the meteorological model used in this study. From Section 2.4.2, it was found that this study overpredicts wind speed compared to the studies that used grid-nudging. Kwok et al. and Liu et al. both used grid-nudging for their meteorological modeling and achieved a better performance in predicting wind speed. Thus, this overprediction of wind—compared to other studies—may be a contributor to the higher negative biases observed for PM concentration prediction. The impact of this negative bias on the prediction of aviation-attributable $PM_{2.5}$ is uncertain, and will remain as a limitation of this thesis work.

3 Background Emissions

A background emissions (non-aviation anthropogenic emissions) dataset, in conjunction with the aviation emissions dataset, is essential to quantifying the air quality impacts of aviation, because it sets the ambient conditions in which aviation emissions enter to go through complex physicochemical processes and form secondary PM. For atmospheric modeling purposes, utilizing a set of emission inputs that reflects the spatial and temporal emission profiles is necessary in achieving agreement between the model and observation concentrations of pollutants. Global-scale emissions inventories, such as Emissions Database for Global Atmospheric Research (EDGAR) [35] and Global Emissions Initiative (GEIA) [36] are utilized in global-scale CTMs.

In comparison to North America and Europe, there are relatively few Asian inventories of anthropogenic emissions available. The development of Asian emissions inventories began with Kato and Akimoto [38] and Akimoto and Narita [39], which reported SO_2 and NO_X emissions in the 1990s. More recently, emissions inventories with a more complete set of air pollutant species were developed for Asia; Streets et al. [40] developed of a recent-year emissions inventory in 2003, followed by its successor, Zhang et al. [41] in 2009. Ohara et al. [42] took a step further to generate Asian anthropogenic emissions for the period 1980-2020, including future year background emissions estimates.

For this thesis, a combination of four emissions inventories—including two regional-scale Asian emissions inventories and two fine-resolution global-scale inventories—are processed to generate the CMAQ-ready background emission files. This chapter discusses the details of the four inventories, the emissions file generation methodology, and the uncertainty of the emissions.

3.1 Emissions Inventories

This section describes the four anthropogenic emissions inventories used for this thesis work. The majority of the inland emissions species comes from Streets et al. [40] and Zhang et al. [41]. A fine-resolution global emissions inventory from PBL Netherlands Environmental Assessment

Agency [43] is utilized for NH_3. Lastly, shipping emissions inventory developed by Corbett et al. [44] is used to capture the shipping emission profiles for the Asian domain.

3.1.1 TRACE-P Emissions

In 2003, Streets et al. [40] developed an emissions inventory for year 2000 that includes SO_X, NO_X, CO, non-methane volatile organic compounds (NMVOC), black carbon (BC), organic carbon (OC), NH_3, and CH_4. This inventory was developed to contribute to the NASA TRACE-P (Transport and Chemical Evolution over the Pacific) Mission [45] and ACE-Asia (Asian Pacific Regional Aerosol Characterization Experiment) [46]. The domain of this dataset stretches from Pakistan in the West to Japan in the East, and from Indonesia in the South to Mongolia in the North; a map of this domain is presented in the next section, as Zhang et al. [41] is developed for the same domain.

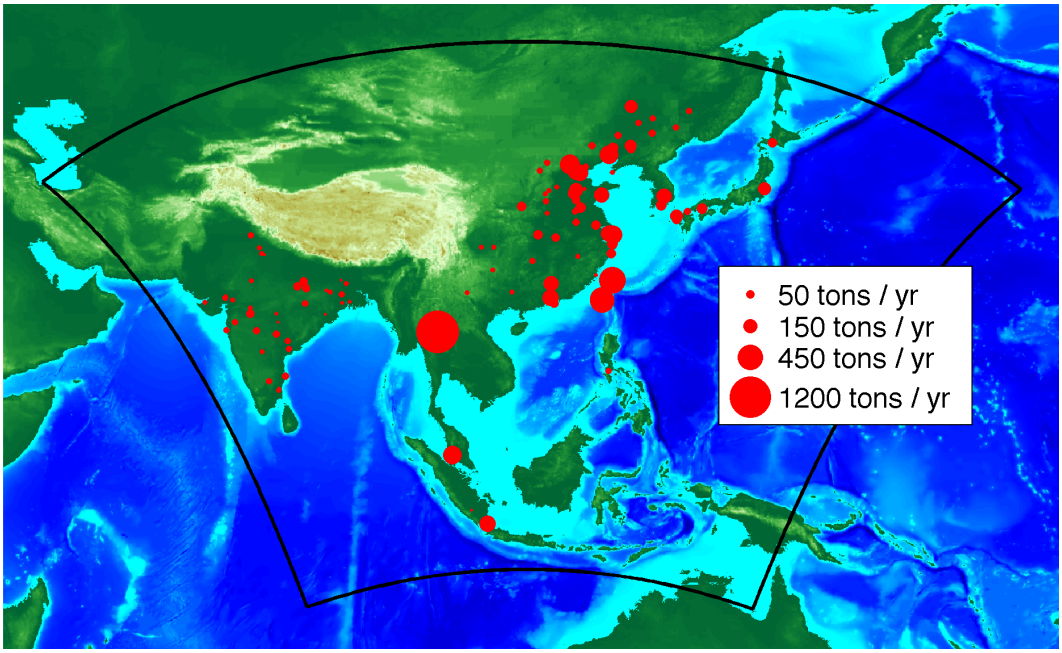

Figure 3-1: Black carbon emissions from TRACE-P large point source locations

There are two components to this emissions dataset: gridded emissions and point-source emissions. Gridded emissions for this inventory has a 1° × 1° horizontal grid resolution; this component is disregarded for this thesis, because a more up-to-date and a finer-resolution set of gridded emissions from Zhang et al. [41], described in the following section. However, this

dataset is needed to obtain the most up-to-date large point source emissions data, which takes into account power plants and some large iron and steel plants included for CO emissions. The locations of these large point sources are determined from the RAINS-Asia (Regional Air Pollution Information and Simulation Asia) [46] and the GEIA inventory [36]. Figure 3-1 presents the locations and the amount of emitted pollutants (black carbon in this case) for 115 large point sources. Other species that are available from this dataset are CO, NMVOC, NO_X, OC, and SO_2. From here on, the point-source emissions dataset obtained from Streets et al. [38] will be referred to as TRACE-P emissions.

3.1.2 INTEX-B Emissions

Zhang et al. [41] presents a new inventory of air pollutant emissions in Asia in the year 2006, following the steps of its predecessor, TRACE-P emissions. This dataset was developed to support the Intercontinental Chemical Transport Experiment-Phase B (INTEX-B) conducted by the National Aeronautics and Space Administration (NASA). Thus, from here on, this dataset will be referred to as INTEX-B emissions.

INTEX-B emissions include particulate matter with diameters less than or equal to 10μm (PM_{10}) and particulate matter with diameters less than or equal to 2.5μm ($PM_{2.5}$), which TRACE-P emissions did not address. Also, the emissions numbers were updated from year 2000 to 2006, since a rapid growth of the economy and energy use in China significantly changed the amount of emitted pollutants; emissions from China are emphasized in INTEX-B, because they represent a significant fraction (between 42% and 66%) of the emissions in Asia. Growth of anthropogenic emissions in China is shown in Table 3-1; a more comprehensive comparison is presented in [41].

	SO_X	NO_X	CO	NMVOC	PM_{10}	$PM_{2.5}$	BC	OC
Growth	36%	55%	18%	29%	13%	14%	14%	14%

Table 3-1: Percentage growth of anthropogenic emissions (annual) in China from 2001 to 2006

The spatial domain of this dataset, which is identical to the domain covered by TRACE-P, is illustrated in Figure 3-2. This domain is covered by 0.5° × 0.5° horizontal grids, which is an improvement from TRACE-P's 1° × 1° resolution.

Figure 3-2: Definition of the inventory domain (for TRACE-P and INTEX-B)

INTEX-B dataset presents an annual sum of the anthropogenic species (SO_2, NO_X, CO, NMVOC, PM_{10}, $PM_{2.5}$, BC and OC) from four different source categories: power generation, industrial production, residential combustion, and transportation (gasoline and diesel vehicles). A further discussion on the emissions from different source categories is presented in Section 3.2.5.

3.1.3 NH_3 (Ammonia) Emissions

Ammonia is an important atmospheric pollutant with a wide variety of impacts, which includes its role in secondary PM formation. Major sources of ammonia emission include livestock production and fertilizer use; large portions of India and China emit a significant amount ammonia from these sources. Thus, an accurate representation of NH_3 emissions in Asia is needed for this thesis work, in order for the model to capture the formation of secondary aerosols in the atmosphere.

Ammonia emissions data is included in the TRACE-P inventory; however, a finer-resolution global emissions inventory is available from PBL (Planbureau voor de Leefomgeving) Netherlands Environmental Assessment Agency [43]. This dataset updates its predecessor [47]

with data for the year 2000 and significantly improves the horizontal grid resolution from 1° × 1° to 5min × 5min. Any reference to ammonia emissions from here on will be directed at this dataset.

The updates in the INTEX-B inventory indicate a significant growth in the amount of pollutants emitted from anthropogenic sources from 2000 to 2006. However, ammonia is not one of the species that were updated from the TRACE-P inventory; Zhang et al. [41] indicates that the amount of NH_3 has not changed significantly since 2000, unlike other species that required updates. This insignificant change in ammonia emissions from 2000 to 2006 is also confirmed by Ohara et al. [42].

3.1.4 Shipping Emissions

Aviation-attributable health impacts are calculated by observing the changes in surface-level $PM_{2.5}$ concentrations and the population that are affected by the change. This method suggests that the pollutant concentrations of grid cells directly above the oceans can be safely disregarded for health impacts calculations. However, emissions that occur over the water (i.e. shipping emissions) should not be ignored; pollutants emitted over the ocean can move into the dry land via transport mechanisms. Studies have shown that ships make a non-negligible contribution to air quality and human health [48-50].

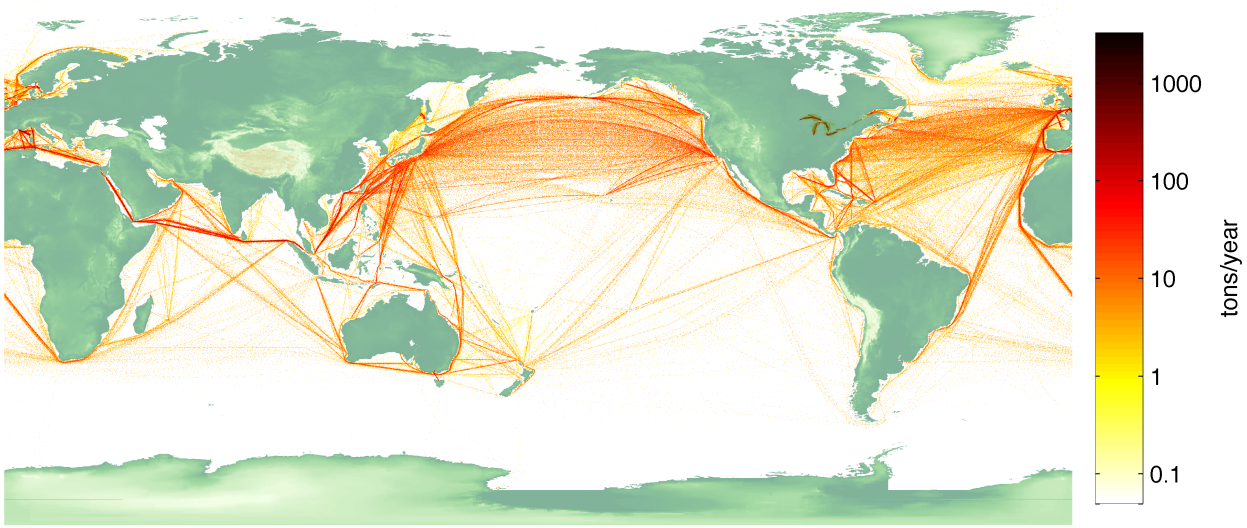

Figure 3-3: Global shipping emissions: NO_X (annual sum)

In order to account for shipping emissions, a global ship emissions inventory developed by Wang et al. [44] is utilized for this thesis work. This inventory has 0.1° × 0.1° grid resolution, and includes monthly emission sums of SO_2, NO_X, CO, BC, NMVOC, and $PM_{2.5}$; this inventory updates emission values based on 2001 data with 2008 to 2010 estimates. This dataset, from here on, will be referred to as shipping emissions.

Figure 3-3 shows annual sum NO_X emissions from the shipping emissions inventory. The plot clearly displays the major shipping trade routes across the oceans. A portion of this global dataset that is within the CMAQ domain is utilized for this thesis work.

A summary of the four datasets described in the previous sections is presented in Table 3-2.

Inventory	Sectors	Source Type	Resolution	Species
Streets et al.	• Power Generation	Point	N/A	BC, OC, NO_X, SO_2, CO, NMVOC
Zhang et al.	• Industrial • Transportation • Residential • Power Generation	Gridded	0.5° × 0.5°	BC, OC, NO_X, SO_2, PM_{10}, $PM_{2.5}$, CO, NMVOC
Beusen et al.	N/A	Gridded	5min × 5min	NH_3
Wang et al.	• Shipping	Gridded	0.1° × 0.1°	BC, NO_X, SO_2, $PM_{2.5}$, CO, NMVOC

Table 3-2: A summary of the four emissions inventories used in this thesis

3.2 Methodology

As described in the previous section, four different emissions datasets are chosen for this study in order to ensure the highest resolution data available for the emissions species of interest. Combining four different inventories, however, adds difficulties in generating CMAQ-ready emissions files; the inventories vary in resolution, temporal scale, pollutant species definitions, and units used. Thus, a set of MATLAB codes were written to process and generate emissions files. This section describes the processes that were taken to generate emissions files for CMAQ.

3.2.1 Horizontal Allocation

The four datasets only define the locations of emission sources in the horizontal domain in their corresponding spatial resolutions. Therefore, the initial step taken to combine the four emissions inventories is horizontal allocation into the CMAQ modeling domain, which—as described in Chapter 2—has 164 rows and 193 columns of 50km × 50km horizontal grids.

The TRACE-P inventory has exact locations of the large point sources; with this information, the emissions are assigned to the CMAQ grids that contain the locations of the point sources. Ammonia emissions and shipping emissions are both gridded and have finer grid resolution compared to the CMAQ grids (approximately 1/6 to 1/5 of the CMAQ grid per dimension). Therefore, the grid centers of the two inventories are observed, and the corresponding emissions are assigned to the CMAQ grids that contain the inventory grid centers. Figure 3-4 illustrates the results of horizontally allocated ammonia emissions.

In order to ensure mass conservation, the emissions sum within the CMAQ domain is calculated for both raw and allocated data. The sums are consistent, as shown on the title lines of Figure 3-4. The spatial patterns of the emissions also remain consistent.

A similar process is applied to the INTEX-B inventory; however, because the grid resolution of this inventory (approximately 55km per dimension) is comparable to the CMAQ grid resolution, an extra step is required beforehand. Each INTEX-B grid is divided equally into 81 squares, along with the corresponding emission values. Then the divided INTEX-B emissions are assigned to the CMAQ grids. The result of this allocation for NO_X emissions from INTEX-B is shown in Figure 3-5. Once again, the spatial pattern of the emissions is approximately consistent; the emission sums also equal to each other.

The horizontal allocation process appropriately assigns all the monthly- (shipping) and annually- (INTEX-B, TRACE-P, and ammonia) summed emissions into the 2-D space defined during the model setup. The next section adds another dimension to the emissions profile by assigning the horizontally allocated emissions into a 3-D space.

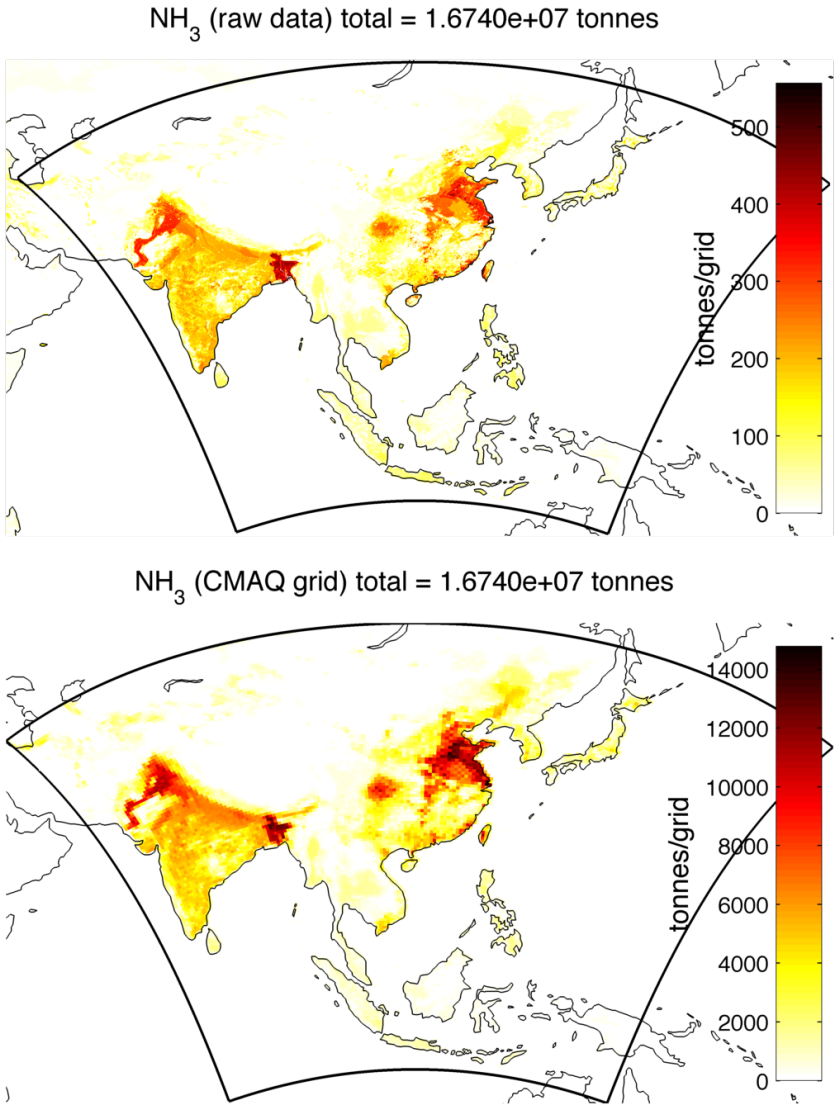

Figure 3-4: Ammonia emissions before (top) and after (bottom) horizontal allocation

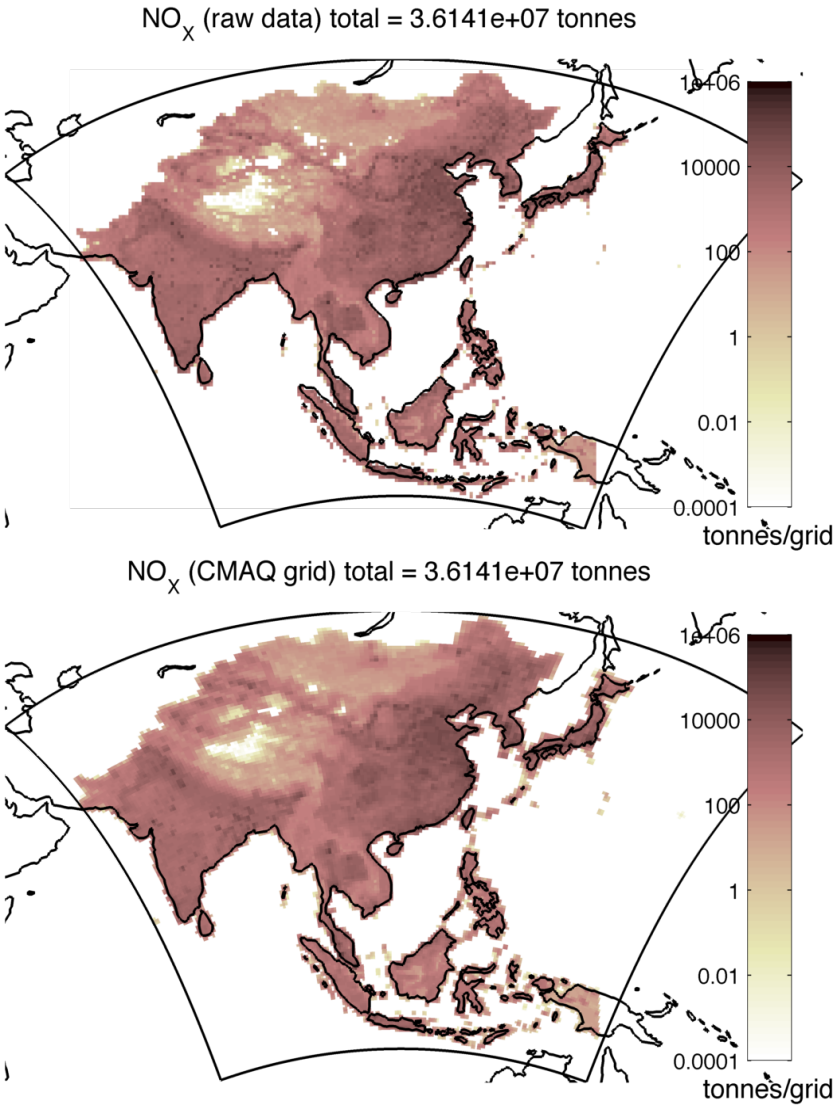

Figure 3-5: INTEX-B NO_X emissions before (top) and after (bottom) horizontal allocation

3.2.2 Vertical Layer Assignment

Anthropogenic emissions such as residential and transportation emissions are emitted near the ground, which can be assigned to the ground-level vertical layer in the modeling domain. However, power plants and large industrial factories emit their by-product pollutants at the top of smokestacks that are designed to alleviate the impact of emitted pollutants to the surrounding region. The effective stack height is not only affected by the physical height of the smokestacks, but also is affected by buoyancy and initial momentum. As a result, large point source emissions must be properly assigned to the appropriate higher vertical layers.

From the horizontal allocation process of the TRACE-P inventory, the amount of pollutants (BC, OC, NO_X, SO_2, CO, NMVOC) emitted from 115 large point sources is assigned to the appropriate CMAQ horizontal grids. However, the gridded emissions data from the INTEX-B inventory also contains up-to-date estimates of power generation emissions of the corresponding species. Therefore, a straightforward addition of the two datasets results in a double counting of power generation emissions. In order to address this issue, the CMAQ grids that contain 115 large point source locations receive special treatment.

The amount of power generation emissions from INTEX-B is compared to the amount of TRACE-P emissions for each power generation grid. If the INTEX-B emissions value is larger than the TRACE-P emissions value, the difference between the two is assigned to the ground-level vertical layer; the TRACE-P value is then assigned to an upper vertical layer using plume-rise calculations described later in this section. If the INTEX-B emissions value is smaller than the TRACE-P emissions value, then only the INTEX-B value is used and assigned to an upper vertical layer; no power generation emission is assigned to the ground level.

The methodology described above is used to determine the amount of power generation emissions to be assigned to upper vertical layers; however, the vertical location of this emission must be determined using plume rise calculations. The Sparse Matrix Operator Kernel Emissions (SMOKE) model [27], an emissions processing software widely utilized for the U.S. domain, performs plume rise calculations using the following methodology described in Equations (3.1-3.3); a detailed description of this methodology can also be found in [7].

Effective stack height	$h = h_s + \Delta h$	(3.1)
Plume rise	$\Delta h = \begin{cases} 21.4 \times F^{0.75} / U_a, & F < 55 \\ 38.7 \times F^{0.60} / U_a, & F \geq 55 \end{cases}$	(3.2)
Buoyancy flux parameter	$F = 0.25 g d^2 V_s (T_s - T_a) / T_s$	(3.3)

Nomenclature for Equations (3.1-3.3):

U_a = ambient velocity at stack height, m/s
g = gravitational acceleration, 9.807 m/s^2
d = stack inner diameter, m
V_s = stack exit velocity, m/s
T_s = stack exit temperature at h, K
T_a = ambient temperature at h, K

Plant	Unit	h (m)	d (m)	T_s (K)	V_s (m/s)
Jingneng	4	210	7 / 4	323	22.4
Datang	8	120	6	353	10.2
Huaneng	4	238	6	323	22.0
Guohua	4	100 / 240	6.2 / 3.8	373	18.8
Jingfeng	2	150	3.7	338	19.6
Huadian	4	165 / 70	4.5 / 4	331 / 387	26.5 / 7.3
Taiyanggong	2	70	4	377	23.2
Caoqio	2	70	4	377	13.2

Table 3-3: Unit and stack parameters of power plants in Beijing [51]

From the tip of smokestacks, waste gases are usually emitted at temperatures above that of the ambient air and are emitted with non-negligible initial momentum. These properties of waste gases, in addition to the physical properties of the smokestacks and the ambient conditions of meteorology, can be used to calculate the effective stack height (h)—the sum of the actual stack height (h_s) and the plume rise (Δh).

Meteorological variables (U_a and T_a) are obtained from the meteorological fields from WRF simulations described in Section 2.3.1. Due to a lack of available information on the smokestack parameters of the large point sources, average values of the available information from Table 3-3 (adapted from Hao et al. [51]) are used.

The above methodology is used for species that are included in the TRACE-P inventory; however, power generation emissions for PM_{10} and $PM_{2.5}$ are only available in gridded form of INTEX-B inventory. A study by Wang et al. [52] derives the vertical profiles for East Asia based on the U.S. EPA NEI99 to allocate power generation emissions to different vertical layers. This study assigns the following percentages of $PM_{2.5}$ (and PM_{10}) emissions into different vertical layers as follows: 5% (5%) below 76m above ground; 45% (55%) between 76m and 153m above ground; 25% (20%) between 153m and 308m above ground; 20% (15%) between 308m and 547m above ground; and 5% (5%) between 547m and 871m above ground. This profile is adapted to assign PM emissions (excluding BC and OC) into the vertical layers of this model setup. BC and OC emissions are assigned to vertical layers using plume rise calculations, since they are included in the TRACE-P inventory.

3.2.3 Temporal Variation

Another dimension considered for background emissions processing is time, as CMAQ-ready emissions input files are required to have one-hour time steps. Because the emissions input require such a fine temporal resolution, it is important to consider temporal variations in emissions for different time scales (from seasonal to diurnal) as well as different sectors. However, many of the temporal profiles required to process Asian emissions are not available. Thus, for this thesis, as much of the available temporal profile information for the Asian domain are utilized; temporal profiles that are not available for the Asian domain are adapted from other regions (i.e. Europe or the U.S.) or kept invariant.

Various temporal profiles that take into account the seasonal variability of different emission sectors are utilized for this study. Pollutant species that are included in the INTEX-B inventory are considered combustion-related, and the corresponding monthly fractions for the residential, power generation, and industrial sector emissions are adapted from Streets et al. [40] and Zhang et al. [53].

Monthly variation for the residential sector is estimated for China by examining the monthly mean temperatures of each province, assuming a dependence of stove operation on provincial monthly mean temperatures. Power generation and industrial sector monthly profiles are

obtained using monthly data on power generation, cement production, and industrial GDP for the period 1995-2004 [54]. The transportation sector lacks a monthly profile for the Asian domain. With this absence of relevant information, other studies have used European monthly profiles and the use was shown to improve air quality simulations over Nanjing [55] and also the entire Asian domain [52]; therefore, an available profile for the European domain from Olivier et al. [57] is used for this thesis work, although the applicability of the European emissions profile to Asia is uncertain.

Ammonia, not considered to be a combustion-related species (except as relates to after-treatment technologies), adapts a different monthly profile presented in Streets et al. [40]. This profile is constructed considering a temperature dependence of emissions of ammonia from animal waste and fertilizer application for agricultural purposes. Beusen et al. [43] reports shipping emissions monthly, so the seasonal variation is already taken into account.

Figure 3-6 displays the six monthly profiles described in this section. As expected, the residential sector puts higher fraction of the annual total to the winter, as lower outdoor temperatures in the winter is expected to increase residential heating. Also, ammonia emissions peak in late spring and early summer, as the profile is developed based on agricultural activities such as animal waste and fertilizer application, which is most active during those months.

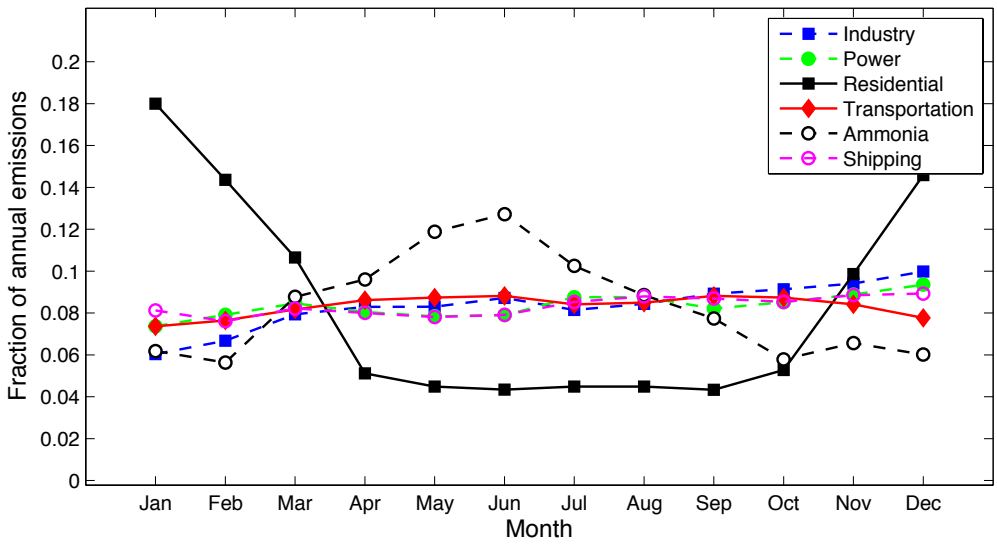

Figure 3-6: Monthly profiles used in this thesis

The day-of-week variation profiles are not readily available for the Asian domain. Wang et al. [52] constructs a profile based on two European emissions inventories. However, it was shown in this study that the impact of this profile based on European data is relatively small; when all sectors combined, the differences of the daytime and nighttime average ground-level emissions resulted from the day-of-week variation are within ±1.5% for all the species, relatively small compared to 13-24% variation due to diurnal variations. For this thesis work, the less-significant day-of-week variation profiles are thus overlooked.

The diurnal variation profiles are also not available for the Asian domain; other studies [52, 55, 58], to compensate for this absence, developed and used profiles based on European emissions inventories. Figure 3-7 shows the diurnal variations profiles that were utilized in those studies. From Figure 3-7(a), power, industry, and residential emissions' diurnal variation profiles are used for this thesis; for the transportation sector, the weekday diurnal variation profiles for the listed pollutant species from Figure 3-7(b) are adapted. Due to a lack of available information, ammonia and shipping emissions are assumed to have a flat (constant) diurnal emission profile.

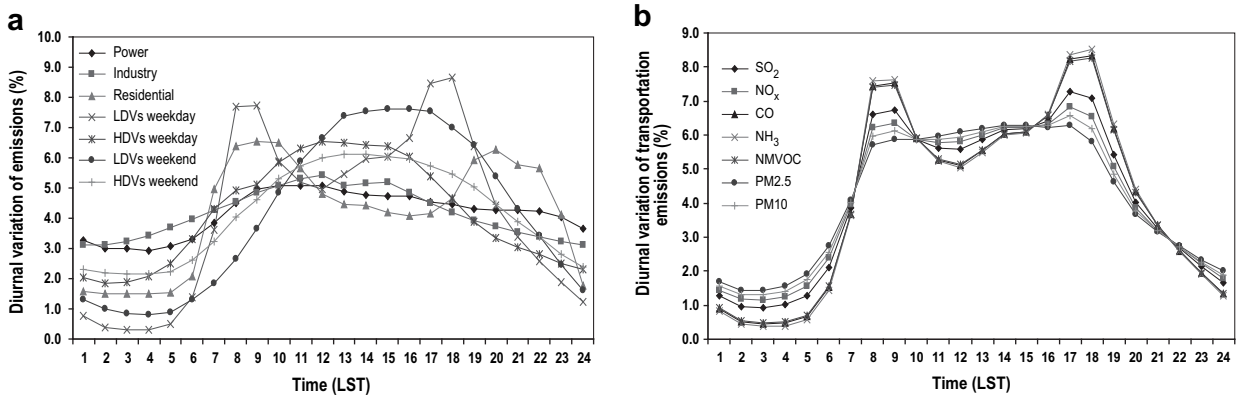

Figure 3-7: Diurnal profiles of various emission sources (a) and weekday transportation emissions (b), [52]

3.2.4 Chemical Speciation

After horizontal allocation, vertical layer assignment, and temporal profile application, a time-variant 3-D emission patterns for the Asian domain is developed; however, the speciation of the pollutants remain the same the raw data inventories. The CMAQ model requires its particulate matter (PM) and non-methane volatile organic compounds (NMVOC) to be appropriately

speciated for the photochemical mechanism used. As described in Section 2.3.2, the Carbon Bond 2005 (CB05) chemical mechanism [29] is used for this thesis work.

However, as data availability over Asia is limited, PM and NMVOC speciation profiles are not available. Therefore, the profiles from the SMOKE model [27] are usually utilized in air quality studies over Asia [21, 59-64]. Recent studies have made efforts to develop similar processing software for Europe [65] and the Pearl River Delta (PRD) region in China [28]. However, the European profile has not been utilized for air quality studies over Asia and the profile for the PRD region is not sector-specific. Thus, this thesis work utilizes the generally used sector-specific profiles from the SMOKE model.

CMAQ 4.7.1 considers particulate matter greater than 2.5μm in aerodynamic diameter as being PMC (for PM Coarse); then CMAQ divides $PM_{2.5}$ into the following species: Primary Elemental Carbon (PEC), Primary Organic Aerosols (POA), Primary Sulfates (PSO_4), Primary Nitrates (PNO_3), and PM_{FINE} (other $PM_{2.5}$ species). The SMOKE model provides a speciation profile for the five species listed; Figure 3-8 illustrates the details of the speciation.

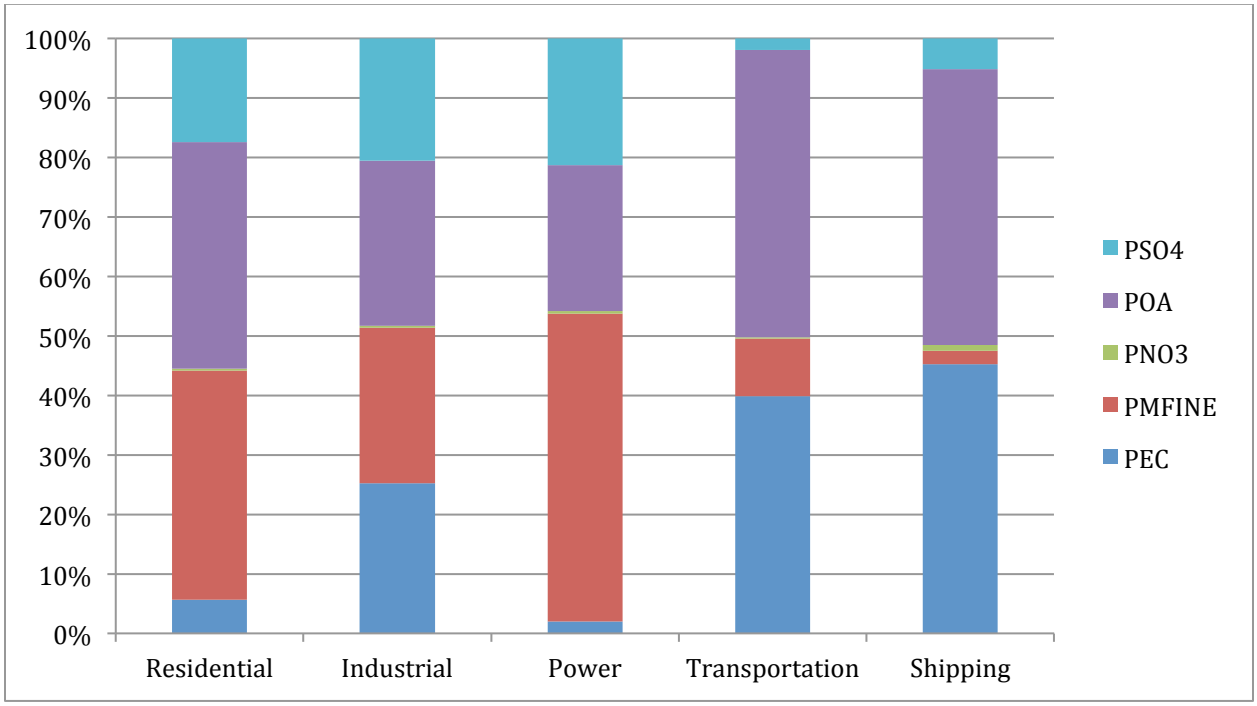

Figure 3-8: $PM_{2.5}$ speciation profiles (percent by mass) from the SMOKE model

For the first four sectors from Figure 3-8, the INTEX-B inventory reports the following particulate matter species: PM_{10}, $PM_{2.5}$, BC, and OC. Therefore, the difference between PM_{10} and $PM_{2.5}$ is assigned to emissions species PMC. BC and OC emission values reported from the INTEX-B inventory are assigned to emission species PEC and POA, respectively; for these two species, the reported values from the emissions inventory takes precedence over the speciation profile from SMOKE, since the inventory values are considered to be more accurate and specific to the Asian domain. Appropriate emission estimates for CMAQ emission species PNO_3, PSO_4, and PM_{FINE} are obtained by applying the speciation profile from SMOKE on $PM_{2.5}$ emission values from INTEX-B. For shipping-attributable $PM_{2.5}$, the speciation profile from SMOKE is utilized for all five CMAQ $PM_{2.5}$ species.

Sector-specific chemical speciation profiles for NMVOC are also obtained from the SMOKE model. Application of these speciation profiles for the five emission sectors resulted in 11 NMVOC lumped species for the CB05 mechanism. A detailed table of the split factors for these lumped species can be found in Appendix C.

3.2.5 Sectoral Emissions

The appropriate spatial allocation, temporal variation, and chemical speciation were applied to the available Asian emission inventories to generate the CMAQ-ready background emission files. For this thesis work, this information on the total background emission is used in conjunction with the aviation emissions dataset to study the health impacts of aviation-specific emissions. The contribution of a certain emission sector (i.e. aviation sector for this thesis) is quantified by comparing simulation results including and excluding the specified emission sector. This impact quantification method can easily be translated into other emission sectors by generating the emission files that exclude various emission sectors, one at a time. In preparation for potential future work, the background emissions files were generated excluding each of the five emission sectors. The results of full-scale CMAQ simulations using these sectoral emission files can be used to quantify the air quality and health impacts of each emission sector; this information may be beneficial for policymakers to consider when developing emissions regulations for Asia. Sector-specific annual sums of combustion-related species for the Asian domain used in this thesis work are presented in Figure 3-9.

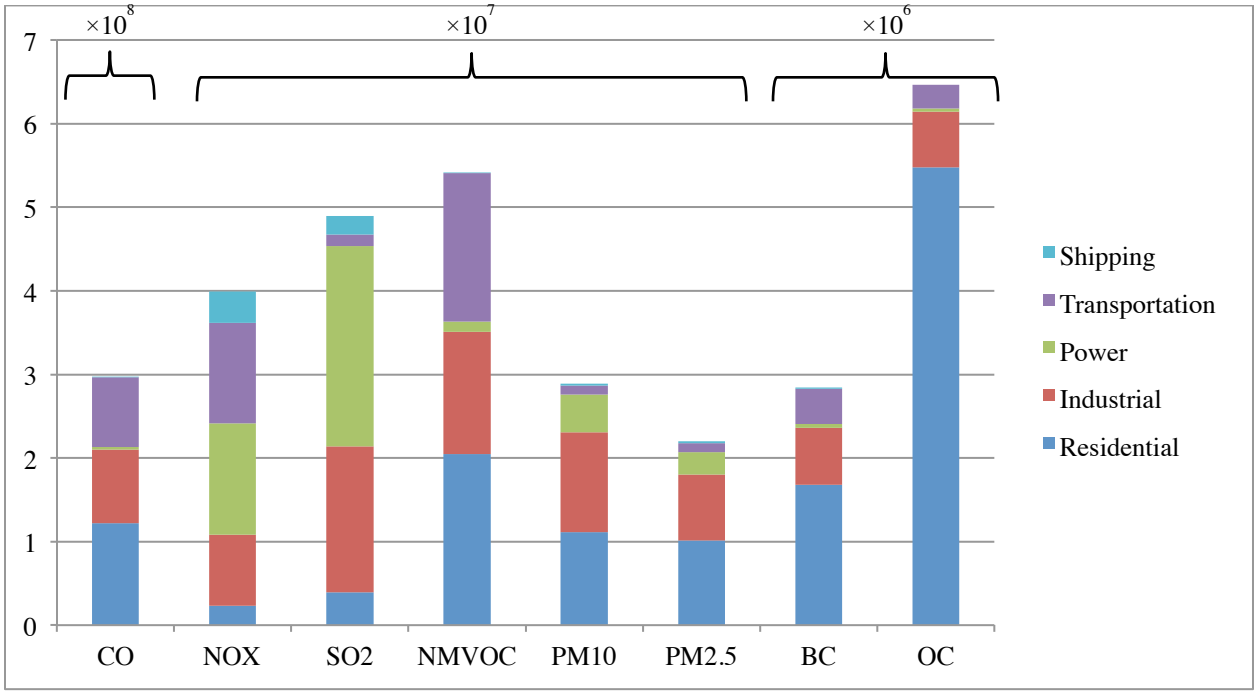

Figure 3-9: Yearly Asian emission of combustion-related species by sector (tonnes/yr)

3.3 Uncertainty in Background Emissions

The emissions inventories used in this thesis work are compiled using the available information on the activity levels and emission factors (i.e. quantity of pollutants that are emitted per unit of fuel used). However, due to a lack of information on reported activity rate, fuel type used, and/or emission factor estimates for Asia, a non-negligible level of uncertainty is innate in the Asian emission inventories.

For example, the INTEX-B inventory—with a significant improvement from its predecessor, the TRACE-P inventory—is still estimated to have the following uncertainty for China measured as 95% confidence intervals: ±12% for SO_2, ±31% for NO_X, ±68% for NMVOC, ±70% for CO, ±132% for PM_{10}, ±130% for $PM_{2.5}$, ±208% for BC, and ±258% for OC [41]. The uncertainties vary by region, as it is expected that the emission estimates for Japan, Korea, and Taiwan—which rely on thorough local level inventories with local knowledge—are to have lower uncertainties compared to those of Southeast Asia, where they lack such local information. Also, the uncertainties vary by emission source; emissions from power generation plants and large

industrial factories are expected to have lower uncertainties, because the activity data and local emission factors are well known. On the other hand, larger uncertainties are expected for emissions from small industries, residential combustion, and vehicles. Thus, the potential future work on sectoral impacts, discussed in Section 3.2.5, must carefully examine the sector-dependent uncertainties; more detailed analyses of the inventories' uncertainties are found in Streets et al. [40] and Zhang et al. [41] for power generation, industry, residential, and transportation sectors. Corbett et al. [66] and Beusen et al. [43] contain uncertainty analyses of shipping and ammonia emissions inventories, respectively.

The significance of background emission uncertainty on the health impacts analysis from this thesis is unknown. However, previous studies [67, 68] have shown that a variation in background emissions can have significant impact on the aviation-attributable ground-level $PM_{2.5}$ concentration. Therefore, it may be beneficial to perform a sensitivity study to quantify this impact. However, this sensitivity analysis requires many more computationally expensive full-scale CMAQ simulations with different background emission values; thus, the impacts of background emission uncertainty is overlooked for the scope of this thesis. However, our assessment of the modeled vs. measured PM concentrations implacably accounts for emissions uncertainty, as this is not separated from uncertainty caused by errors in meteorology or errors caused by modeling inaccuracies.

4 Aviation Emissions

Aviation-attributable changes in the atmospheric pollutant concentrations are quantified by observing the difference between simulation results of the background scenario and an aviation-included scenario. In order to model the aviation-included scenarios, a global aviation emissions inventory is assigned to the CMAQ modeling domain. This chapter describes the methodologies behind the global aviation emissions inventory utilized in this study, and the CMAQ-ready aviation emissions file generation.

4.1 Aviation Scenarios

This thesis aims to quantify the aviation-attributable air quality and health impacts for four different aviation scenarios. First scenario (Simulation #1) considers aircraft emissions at all altitudes; this scenario is the closest model to how much aviation emissions are generated in the real world, and is simulated to gain the most complete understanding of regional-scale impacts of aviation emissions. The second scenario (Simulation #2) considers the landing and takeoff (LTO) emissions only; this scenario is chosen to follow current regulatory practice, which neglects the effects of aircraft cruise emissions on surface air quality [69, 70]. The third and fourth scenarios (Simulation #3 and #4, respectively) are similar to the first two scenarios; the only difference is that these simulations reflect the usage of ultra-low sulfur (ULS) jet fuel. The descriptions of LTO cycles and ULS fuel are elaborated in the next few sections. Table 4-1 is a summary of the five simulations (one background and four aviation scenarios) performed for this thesis work.

Simulation #	Description	LTO	Cruise	ULS
0	**Background**	✖	✖	**N/A**
1	**Baseline, Full Flight**	✔	✔	✖
2	**Baseline, LTO-only**	✔	✖	✖
3	**ULS fuel, Full Flight**	✔	✔	✔
5	**ULS fuel, LTO-only**	✔	✖	✔

Table 4-1: Different modeling scenarios simulated in this thesis

The results of these five simulations are used to determine the regional-scale health impacts of aviation in Asia; Chapter 5 presents these results, and compares the quantified regional-scale impacts to the numbers obtained from the respective global-scale analyses [8,10].

4.1.1 Landing and Takeoff (LTO) Emissions

Traditionally, aviation emissions have been regulated only for the LTO cycles of flight [71]; the reason behind this practice is that the air quality of airport-surrounding regions is affected primarily by aviation emissions within the atmospheric mixing layer (or planetary boundary layer—PBL). The emitted pollutants—including particulate matter—within the PBL can be transported to the surface layer due to turbulent eddies and vertical motion of the air present in this layer [7].

Several modes of flight are considered for the emissions in the LTO cycle; the modes include ground idle, ground taxi, takeoff, climb-out and descent. These modes, by definition, are operations at or below 3000ft in altitude. However, the way this cutoff altitude is defined requires clarification.

Both above ground level (AGL) and above the field elevation of the airport (AFE) definitions have been used to determine the LTO cutoff altitudes, although the two definitions are not always interchangeable. Geographic features around airports that produce changes in elevation can cause a discrepancy between the AGL and AFE definitions. In the presence of a cliff, for example, the emissions near the airport could be underestimated if the AGL definition is used; this underestimation occurs due to the fact that the AGL altitude jumps as the aircraft passes over the cliff. Thus, in the presence of a cliff, the aircraft spends less time in the LTO cycle by AGL criterion, compared to the AFE criterion. In the presence of a mountain, on the other hand, the aircraft spends more time in the LTO cycle by AFE criterion. Thesis work by Ashok [68] describes this discrepancy using Figure 4-1.

For this thesis work, the AFE definition is implemented for aviation emissions processing. Although the FAA defines LTO as 3000ft AGL, the AFE definition is consistent with the method

in the FAA's Emissions Dispersion and Modeling System [73], required by the FAA in regulatory air quality modeling.

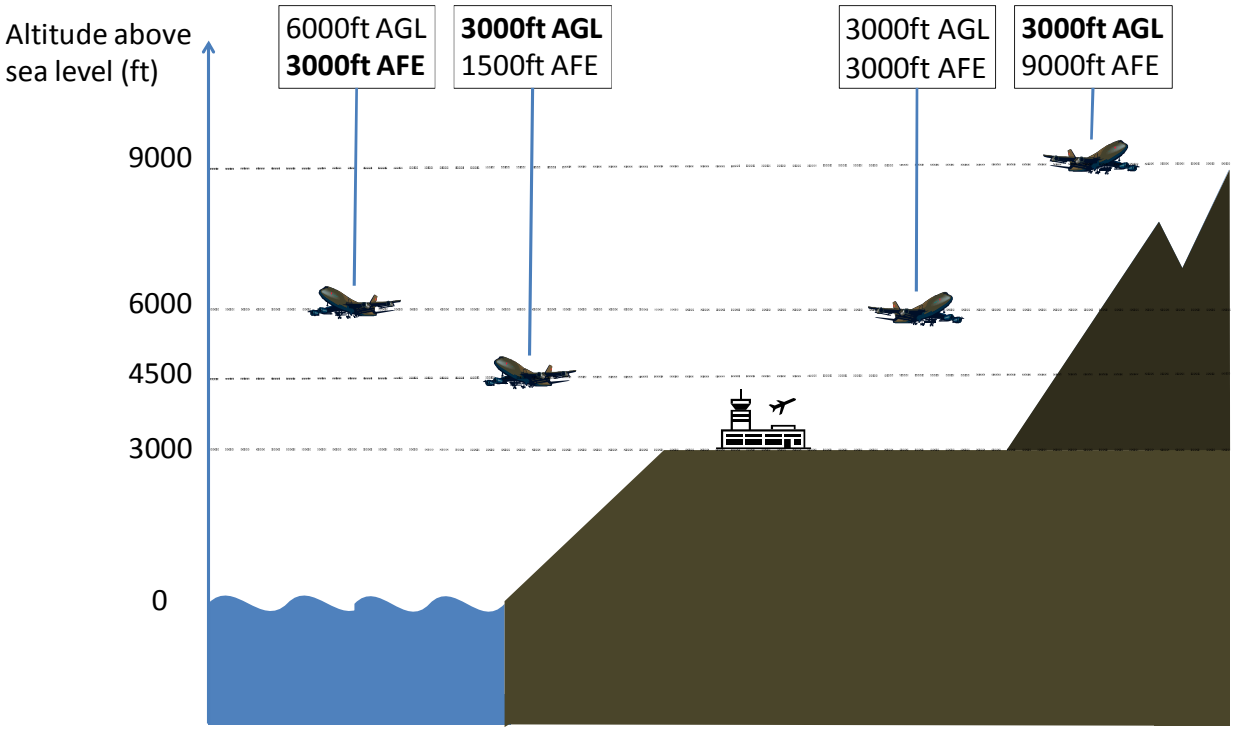

Figure 4-1: Altitude above ground level (AGL) vs. above field elevation (AFE) [68]

4.1.2 Ultra Low Sulfur (ULS) Fuels

In 2006, average fuel sulfur content (FSC) of the fuels used for aviation was between 550 and 750 ppm (by mass) [74], which is below the regulatory limit of 3000 ppm [75, 76]. In 2006, the United States introduced an ultra-low sulfur standard for highway diesel of 15 ppm. In addition, many countries including Australia, Canada, New Zealand, Mexico, Japan, India, Argentina, Brazil, Chile, Peru, and the European Union all have instituted fuel sulfur standards of 50 ppm or less, effective by 2016 for road transportation. With this restriction, utilization of a low sulfur content fuel for aviation may be imminent. Therefore, following the policy case studied by Barrett et al. [8], the regional-scale impacts of utilizing an ultra-low sulfur fuel of 15 ppm, compared to an adopted nominal value of 600 ppm for civil aviation, is studied in this thesis work.

4.2 AEDT 2006

For this thesis work, an emissions inventory generated by the FAA's Aviation Environmental Design Tool (AEDT) [77] is utilized to compute aircraft emissions. AEDT converts flight track segment data into fuel burn estimates by using aircraft takeoff gross weight and its performance characteristics. Each flight segment data contains information including aircraft location (i.e. latitude, longitude, and altitude), its speed and track distance, ambient temperature and pressure, and emission mode, which then is used for the estimation of fuel burn. The fuel burn estimates are modeled in space and time, and are used in conjunction with Emission Indices (EIs) in order to estimate the amount of various emitted species. Some of the species that are presented in the AEDT are the following: CO, HC (Hydrocarbons), NO_X (NO, NO_2, and HONO), PMNV (non-volatile PM), and PMFO (fuel organics PM). Estimation methods of the EIs for these species are described in detail in previous studies [68, 78, 79].

4.2.1 Assignment to the CMAQ Grids

The flight track segment data from AEDT are used to generate the CMAQ-read aviation emission files. This emission processing methodology is composed of two steps: spatial and temporal assignment to the CMAQ modeling domain, and derivation of emissions for pollutant species that are compatible with the CMAQ model.

Since AEDT is a global dataset, the flight track segments that are outside the CMAQ modeling domain are neglected. Also, to ensure that aviation activity is modeled appropriately in the CMAQ domain, "flight IDs" from AEDT are used to determine whether the resolution of the segment data from AEDT is fine enough. All the segments from a specific flight are first observed; each segment's latitude, longitude, and altitude are used to assign the segment's location into a specific CMAQ modeling grid; however, the location of the next segment from the same flight is also observed. This practice is done to ensure that the neighboring segments are also assigned to the same or the neighboring CMAQ grids. If this is not the case, then the distance traveled in a single segment is considered too coarse; in this case, the segment is divided into a multiple of shorter segments with the emissions equally divided and assigned to the corresponding sub-segments. The following figures demonstrate the results of horizontal and vertical allocation of aviation emissions from AEDT.

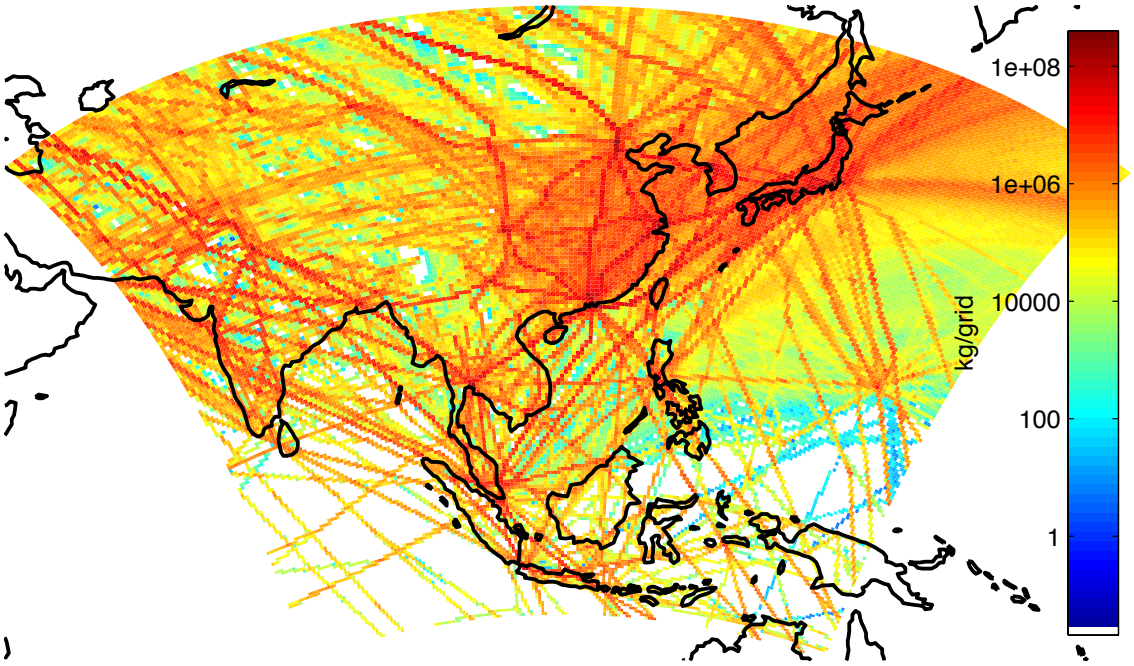

Figure 4-2: A vertical sum of fuelburn (in kg) in the modeling domain for 2006

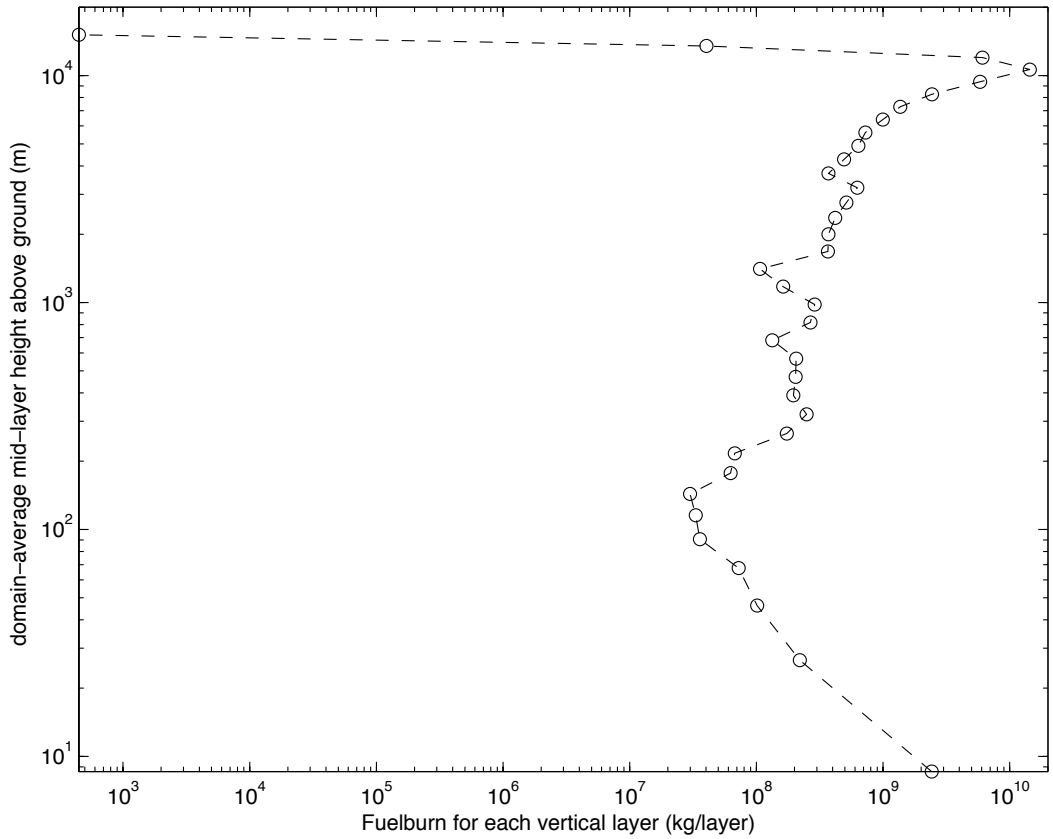

Figure 4-3: Amount of fuelburn (in kg) allocated in each vertical layer for 2006

The vertical layer assignment of aviation emissions is presented in Figure 4-3. Two peaks can be observed from this figure: one at Layer #1 (ground-level), and one at Layer 33 (approximately 10 km above ground); the two peaks respectively represent where the majority of LTO and cruise emissions are assigned. Another feature observed from this figure is that approximately half of the aviation emissions are assigned to layers higher than Layer #33. This significant amount of emissions assigned to upper vertical layers may not have local impacts; however, as this study aims to analyze the regional-scale impacts, the inclusion of aircraft cruise emissions is necessary. The time at the beginning of each segment is also found in AEDT; thus, the time difference between two neighboring segments is used to assign the appropriate amount of emissions from each segment to the correct temporal grid.

The amount of AEDT emissions assigned to the CMAQ modeling domain for the entire year of 2006 is presented in Table 4-2. The Asian emission values are compared to the global aviation emission estimates from AEDT.

	FB (kg)	CO (g)	HC (g)	NO_X (g)	BC (g)	OC (g)
Asia	4.07×10^{10}	1.15×10^{11}	1.88×10^{11}	6.29×10^{11}	1.27×10^{9}	1.18×10^{9}
Global Total	1.88×10^{11}	6.76×10^{11}	9.76×10^{11}	2.67×10^{12}	6.81×10^{9}	1.35×10^{11}
Asia / World	0.22	0.17	0.19	0.24	-	-

Table 4-2: Domain sum of AEDT emissions for Asia and the whole world ("Asia/World" fractions for BC and OC not calculated, due to different methodology used for Asia)

After the AEDT emissions are assigned to the correct spatial and temporal grids, the amount of CMAQ input pollutant species are derived from the emissions data from AEDT. AEDT already contains emission information of CO. NO_X emissions are reported on a NO_2 mass basis. According to the modeling guidance document [77], this emissions estimate contains three species: NO, NO_2, and HONO. (Note that although HONO is not a NO_X species, a fraction of NO_X emissions is assigned to HONO emissions). The suggested partitioning of mole fractions is as follows: 90% NO, 9% NO_2, and 1% HONO for non-LTO emissions, or 76% NO, 23% NO_2, and 1% HONO for LTO emissions; this partitioning is utilized for this thesis.

HC emissions from AEDT are reported on a CH_4 mass basis. Thus, a conversion factor of 1.16 is multiplied to represent HC as total organic gases. Then, the hydrocarbon speciation profile for aircraft engines generated by the FAA and the EPA in 2009 [80] is utilized to assign hydrocarbon emissions into the CB05 lumped species used in CMAQ. The split factors determined for the CB05 lumped species are found in Appendix D.

Black carbon aerosol emissions are computed differently for LTO and non-LTO emissions. For segments that are in the LTO cycle, the reported values of PMNV (in grams) are used. For non-LTO emissions of black carbon, a multiplicative factor of 0.03 is used to convert fuelburn (in kg) into black carbon emissions (in grams); this multiplicative factor is computed using the obtained EI values. Organic carbon aerosol emissions are computed similar to black carbon emissions. Instead of PMNV for LTO black carbon emissions, the values of PMFO are used for LTO organic carbon emissions. The same multiplicative factor of 0.03 is used to compute non-LTO organic carbon emissions.

Several factors are considered when computing the estimates of SO_X (SO_2 and PSO_4) emissions. A fuel sulfur content (FSC) value of 600 ppm (by mass) is considered for the nominal fuel scenarios; FSC value of 15 ppm is considered for the ULS fuel scenarios. Also, a mole fraction value (E = 2%) is used to partition fractions of fuelburn into the respective SO_X species. The guidance document suggests that 2% of the fuel sulfur be modeled as being emitted as PSO_4, and the rest (100% – E = 98%) be modeled as being emitted as SO_2. The following formulas determine the amount of PSO_4 and SO_2 using the AEDT estimates of fuelburn:

For PSO_4: $$\mathrm{PSO_4} = \frac{\mathrm{FSC}}{1000} \times \frac{\mathrm{E}}{100} \times \mathrm{Fuelburn} \times \frac{96}{32} \tag{4.1}$$

For SO_2: $$\mathrm{SO_2} = \frac{\mathrm{FSC}}{1000} \times \frac{100-\mathrm{E}}{100} \times \mathrm{Fuelburn} \times \frac{64}{32} \tag{4.2}$$

The last fraction constants presented in both Equations (4.1) and (4.2) convert the amount of sulfur present in the fuel into the corresponding species by using molar masses of S (32g/mol), SO_2 (64g/mol), and SO_4 (96g/mol).

4.2.2 Uncertainty in the Aviation Emissions

Since the emissions estimates from AEDT are derived from various Emissions Indices that contain uncertainty ranges, the emission files generated using AEDT inherit the propagated uncertainty. Uncertainty estimates for the 2006 AEDT emissions are derived from the uncertainty quantification performed by Stettler et al. [81] for LTO emissions in UK airports. Stettler performs a Monte-Carlo simulation using 2000-member ensembles, with probabilistic distributions on various emissions characterization parameters (i.e. fuel flow, thrust settings, etc.) and emissions parameters (EIs, FSC, etc.). The results of the Monte-Carlo simulation are given as the relative range between 5th and 95th percentile (as percentage of the median), and are presented in Table 4-3.

Species	5th Percentile range	LTO Emissions	95th Percentile range
NO_X (in kg NO_2)	(-26%)	8.19×10^6	(+36%)
SO_2 (in kg)	(-29%)	6.26×10^5	(+33%)
PSO_4 (in kg)	(-56%)	2.29×10^4	(+89%)
CO (in kg)	(-47%)	1.04×10^7	(+87%)
HC (in kg CH_4)	(-66%)	1.57×10^6	(+173%)
BC (in kg)	(-49%)	1.45×10^5	(+75%)
OC (in kg)	(-66%)	2.00×10^4	(+72%)

Table 4-3: UK airport LTO emissions with uncertainty ranges as percentage of the median

Uncertainty ranges quantified by Stettler can be used to estimate the possible uncertainty ranges for the aviation emissions generated for Asia. However, since this study focuses on the LTO emissions at UK airports, the quantified values must be utilized for this study with caution, since this thesis includes cruise emissions and models the Asian domain.

5 Results

This chapter presents the results of CMAQ simulations performed to quantify the air quality impacts of aviation in Asia. The CMAQ simulations described in this chapter follow the preparation processes described in Chapters 2 to 4; the five simulations that were performed will be referred to as Simulation #0-#4, consistent with the descriptions from Table 4-1. Furthermore, this chapter describes the health impacts quantification methodology used to estimate the number of premature mortalities attributed to aviation in Asia. Then, the estimated health impacts results are presented, with comparisons to the global-scale results of previous studies.

5.1 Air Quality Impacts

As an intermediate step to determining the health impacts of aviation, the aviation-attributable air quality impacts are first quantified. For this purpose, aviation-attributable changes in surface level concentration of $PM_{2.5}$ are considered, since long-term exposure to $PM_{2.5}$ species is strongly linked to adverse health risks and mortalities [5]. The air quality impacts are quantified by taking the annual average concentration of $PM_{2.5}$ for each of the five CMAQ simulations, then subtracting the background simulation results from the four aviation scenario simulation results. For this thesis work, all primary PM species and inorganic secondary PM species are considered.

5.1.1 Constituents of $PM_{2.5}$

The CMAQ model used in this study outputs hourly concentrations of 136 chemical pollutants; the species of interest for this study include inorganic aerosols (sulfates: ASO4, nitrates: ANO3, and ammonium: ANH3), primary organic aerosol compounds (AORGP), and elemental carbon (also known as black carbon, AEC). CMAQ also outputs these particulate matter species according to three distinct modes of aerosol formation: Aitken (I), accumulation (J), and coarse (K) [82]. Only the 'I' and 'J' modes of the pollutant species are included for $PM_{2.5}$ calculations.

For the four aviation scenario simulations, annual (temporally) and domain (spatially) average concentrations of aviation-attributable $PM_{2.5}$ species are calculated to see the magnitude of domain-wide aviation impact; also, the composition of aviation-attributable $PM_{2.5}$ from different

aviation scenarios are compared to observe the specie-specific impacts. The domain-average annual $PM_{2.5}$ values are presented in Figure 5-1.

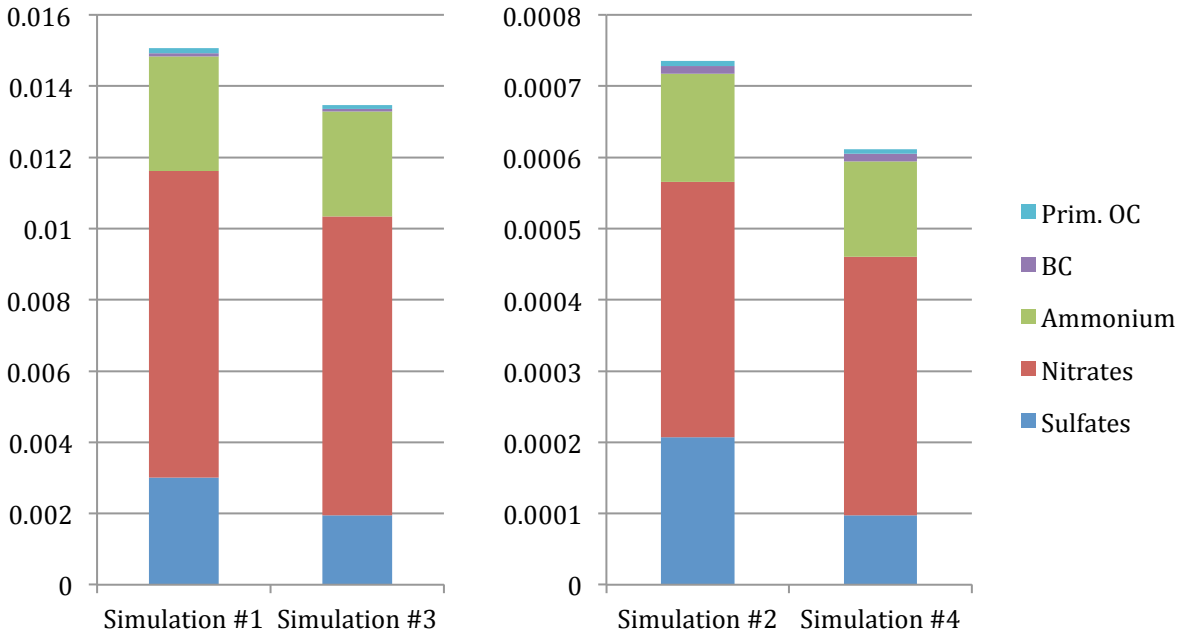

Figure 5-1: Aviation-attributable domain-average annual $PM_{2.5}$ ($\mu g/m^3$)

On the left from Figure 5-1, the two full flight simulations (#1 and #3) are compared. A decrease in the amount of aviation-attributable sulfate aerosols is clearly visible as a result of ULS fuel implementation. On the right from Figure 5-1, the two LTO simulations (#2 and #4) are compared, and a similar pattern is observed. Notice that the domain-average aviation $PM_{2.5}$ is approximately 20 times larger in full flight scenarios compared to the results of LTO-only scenarios.

5.1.2 Spatial Distribution of Aviation-Attributable $PM_{2.5}$

For this thesis work, the spatial variation in the aviation-attributable $PM_{2.5}$ concentration is important since the health impacts depend on the population affected by the pollutant concentration perturbations at the respective locations. Figures 5-2(a)-(d) illustrate the spatial variation in aviation-attributable annual $PM_{2.5}$ concentrations; notice that the color scales used in Figures 5-2(a) and 5-2(c) are different from those of Figures 5-2(b) and 5-2(d).

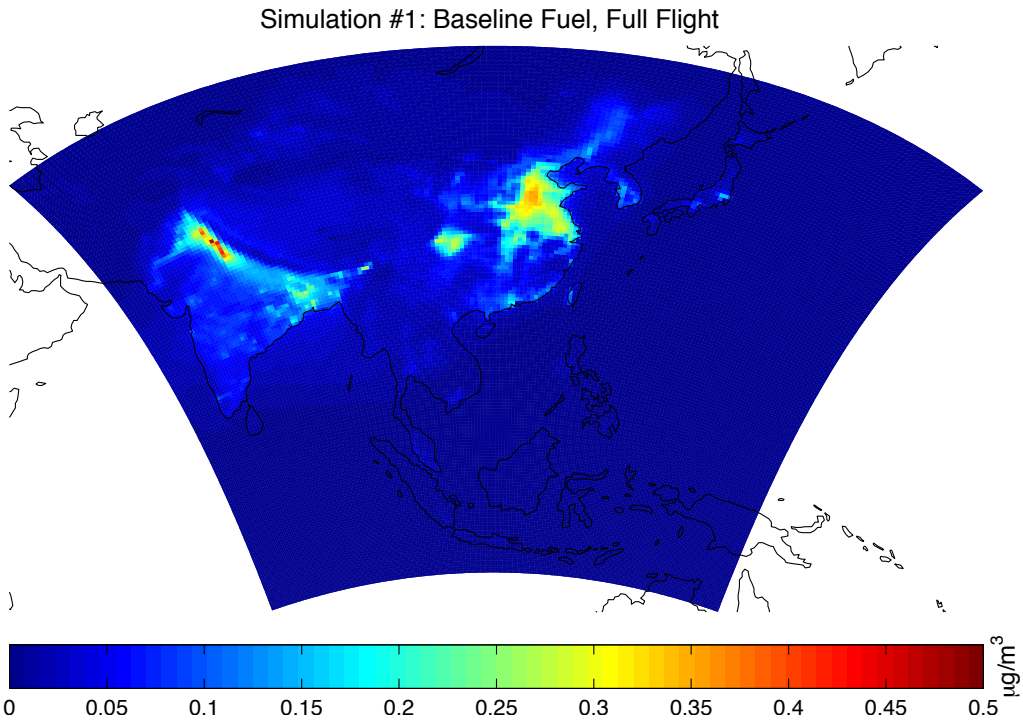

Figure 5-2(a): Change in annual average $PM_{2.5}$ concentration due to aviation in Simulation #1 (Baseline Fuel, Full Flight)

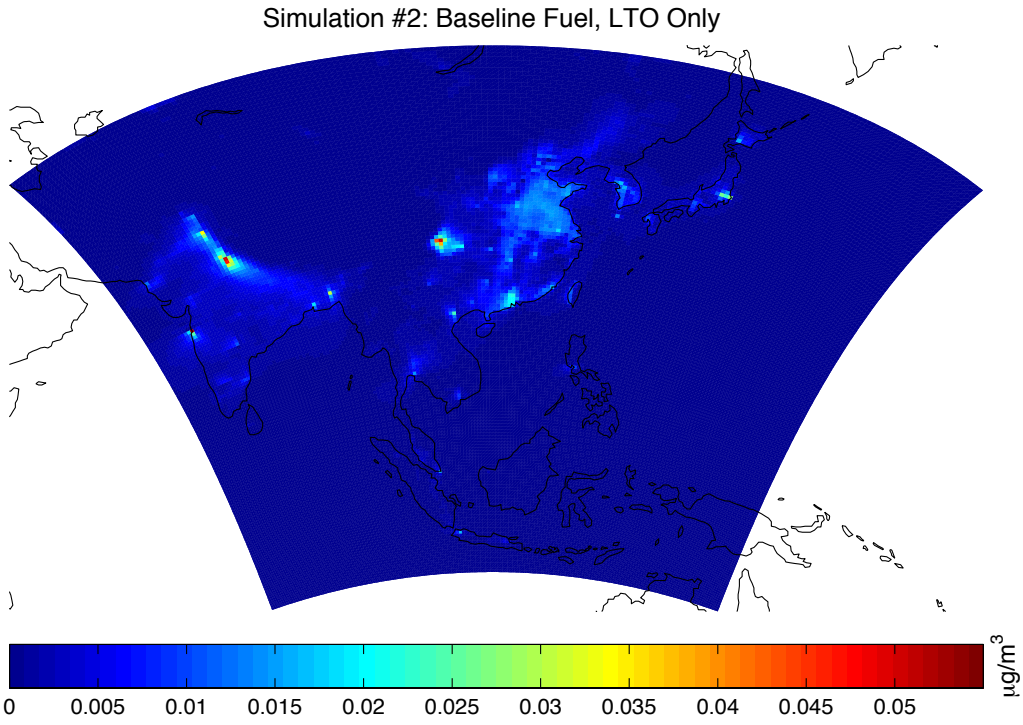

Figure 5-2(b): Change in annual average $PM_{2.5}$ concentration due to aviation in Simulation #2 (Baseline Fuel, LTO Only)

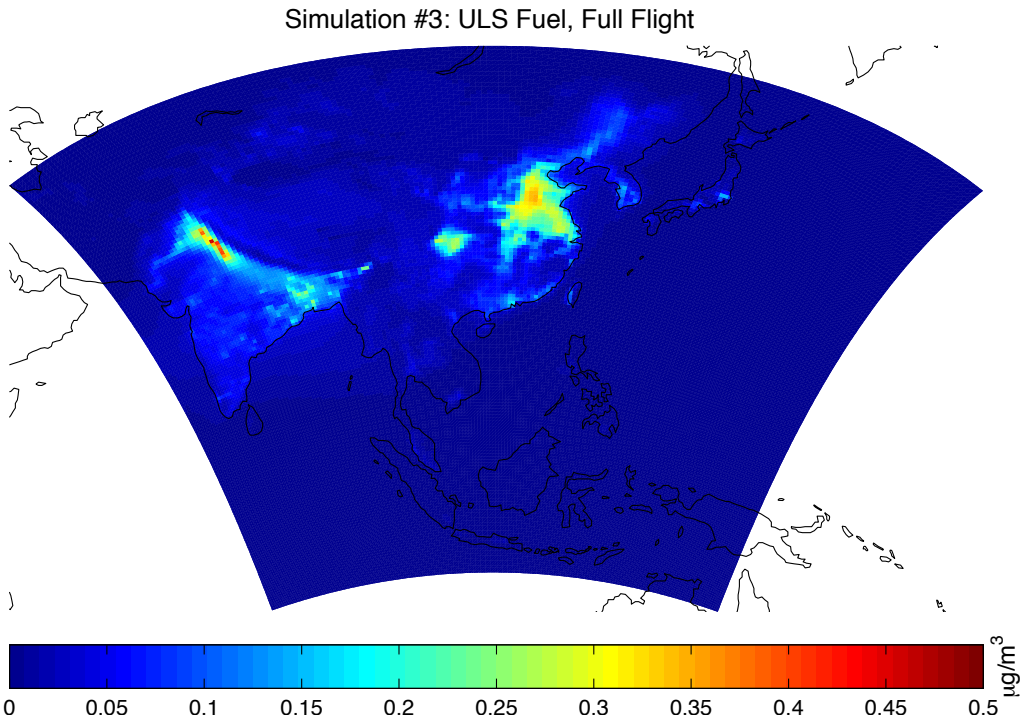

Figure 5-2(c): Change in annual average $PM_{2.5}$ concentration due to aviation in Simulation #3 (ULS Fuel, Full Flight)

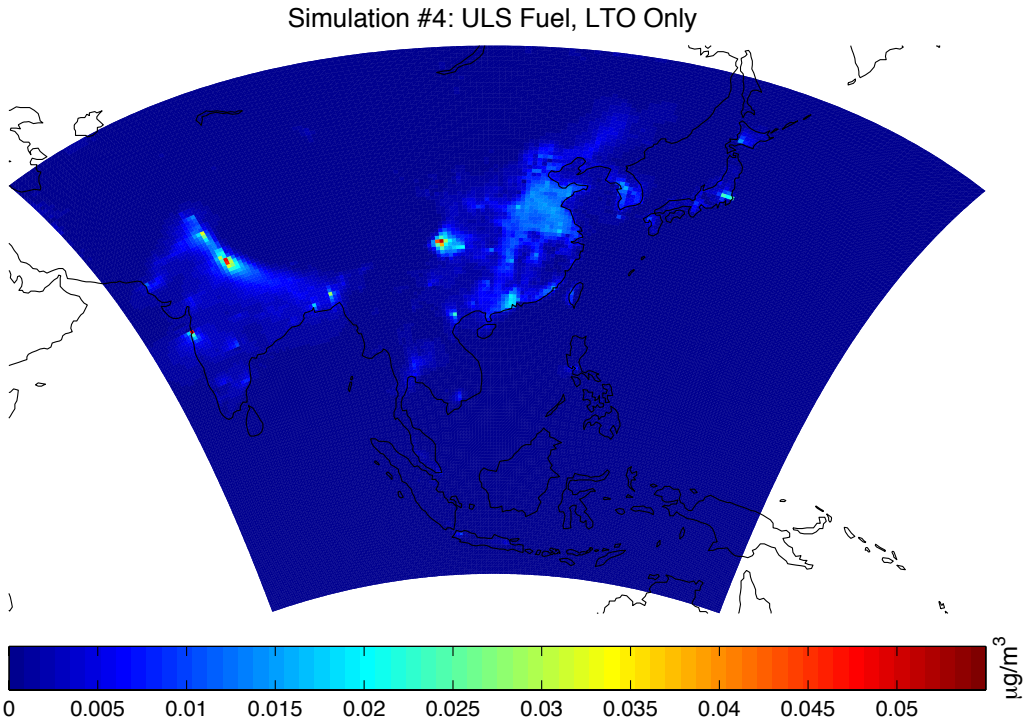

Figure 5-2(d): Change in annual average $PM_{2.5}$ concentration due to aviation in Simulation #4 (ULS Fuel, LTO Only)

The difference between spatial patterns of aviation-attributable $PM_{2.5}$ from full flight scenarios and those of LTO-only scenarios is evident. Figures 5-2(a) and (c), which represent the results of full-flight scenarios, have a wider area coverage of aviation $PM_{2.5}$ compared to the area coverage of LTO-only impacts represented in Figures 5-2(b) and (d); this result is consistent with the global-scale model simulation results from Barrett et al. [10]. Also, consistent with the global-scale model results, the high aviation $PM_{2.5}$ concentration areas are located in Eastern China and Northern India regions; this spatial pattern is also in agreement with the aviation emission pattern observed from Figure 4-2.

5.2 Health Impacts

In this section, the description of the health impacts quantification methodology is presented. Then, using the air quality impact results from the previous section, the number of premature mortalities attributable to aviation is quantified and compared to the global-scale modeling results.

5.2.1 Health Impacts of $PM_{2.5}$ Exposure

Previous epidemiological studies showed a correlation between long-term population exposure to $PM_{2.5}$ and increased risk of health impacts in the U.S. and elsewhere [83-89]. Compared to other health impacts, premature mortality dominates when monetized health endpoints in benefit-cost analyses are considered [90]. Thus for this thesis work, the health impacts are quantified using the number of premature mortalities attributable to aircraft emissions. Health impacts due to long-term population exposure to $PM_{2.5}$ are largely from cardiovascular diseases, respiratory diseases, and lung cancers, although lung cancer risk due to $PM_{2.5}$ exposure is not as well characterized [91]. Supported by evidence presented by the epidemiological studies mentioned, premature mortalities resulting from cardiopulmonary diseases and lung cancer are considered for this thesis.

A Concentration Response Function (CRF) defines the link between $PM_{2.5}$ concentration perturbations and corresponding health impacts. Studies have indicated that a linear association best fits the relationship, and all concurred that this fit holds within the range of concentrations observed in those studies. However, the slope of this linear CRF may not be the same throughout

a wider range of concentrations observed globally: for example, prior work by the WHO in global burden of disease modeling used a log-linear CRF to account for lower slope at higher concentrations. Therefore, in order to make fair comparisons to global-scale studies that used different types of CRFs, both a linear CRF—following current EPA methodology [90]—and a log-linear CRF—from the WHO health impacts methodology [89]—are both utilized, resulting in two sets of premature mortality numbers. Equations (5.1-5.2c) describe the CRF formulations:

$$\text{EPA:} \quad \Delta(\text{Premature Mortalities}) = \sum_{i,j} P_{(i,j)} \cdot (\beta_k^{CP} \cdot B_k^{CP} + \beta_k^{LC} \cdot B_k^{LC}) \cdot (\chi_{av} - \chi_{bg}) \qquad (5.1)$$

$$\text{WHO:} \quad \Delta(\text{Premature Mortalities}) = \sum_{i,j} \left(\frac{RR_k^{CP}-1}{RR_k^{CP}} \cdot B_k^{CP} + \frac{RR_k^{LC}-1}{RR_k^{LC}} \cdot B_k^{LC}\right) \cdot P_{(i,j)} \qquad (5.2a)$$

$$RR_k^{CP} = \left(\frac{\chi_{av}+1}{\chi_{bg}+1}\right)^{\alpha_k^{CP}}; \quad RR_k^{LC} = \left(\frac{\chi_{av}+1}{\chi_{bg}+1}\right)^{\alpha_k^{LC}} \qquad (5.2b,c)$$

The following nomenclature are used for equations above: *k* denotes the country of interest; *(i,j)* is the horizontal grid index pair; $P_{(i,j)}$ denotes the population above 30 years of age in grid *(i,j)*; β is the disease-specific fractional increase in mortality given one μg/m^3 increase in annual average $PM_{2.5}$; *B* is the disease-specific baseline per capita mortality rate in a specific country; χ_{av} and χ_{bg} are grid-specific $PM_{2.5}$ concentration for aviation and background scenarios, respectively; α denotes a disease-specific exponent. The population data from Global Rural-Urban Mapping Project (GRUMP) [92], utilized for this thesis work, is illustrated in Figure 5-3.

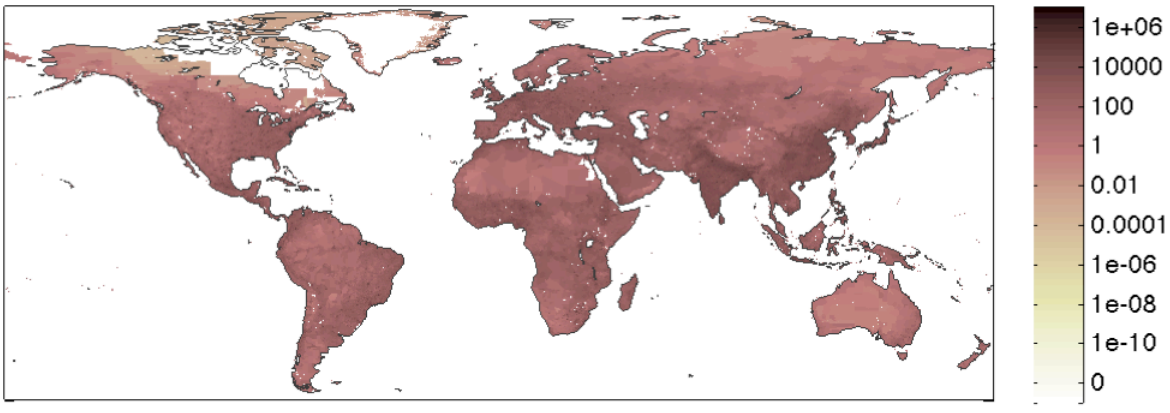

Figure 5-3: Gridded population data from GRUMP (units: population per 2.5min grid)

The disease-specific baseline incidence rates (B) are computed using the WHO Global Burden of Disease (GBD) database [93]. The β values are obtained using the methodology described in [9]: $\beta^{CP} = 0.01$ and $\beta^{LC} = 0.015$ (β^{LC} can range from 0.005 to 0.026). The α values are obtained from [11]: $\alpha^{CP} = 0.15515$ (95% confidence interval: [0.05624, 0.2541]) and $\alpha^{LC} = 0.23218$ (95% confidence interval: [0.08563, 0.37873]).

5.2.2 Premature Mortality Results

Using the methodology described in Section 5.2.1, the number of premature mortalities attributable to aviation is calculated for each of the four aviation scenarios. The estimated numbers of premature mortalities are presented in Table 5-1.

	Simulation #1 (Full Flight, Normal Fuel)	Simulation #2 (LTO Only, Normal Fuel)	Simulation #3 (Full Flight, ULS Fuel)	Simulation #4 (LTO Only, ULS Fuel)
Total	9390 (6420)	550 (390)	8900 (5930)	510 (340)
China	4570 (1730)	260 (100)	4420 (1650)	240 (90)
India	3460 (3180)	190 (170)	3220 (2920)	170 (160)
Bangladesh	450 (250)	30 (10)	420 (230)	30 (10)
Pakistan	420 (280)	20 (10)	400 (260)	20 (10)
Japan	160 (280)	20 (50)	140 (250)	20 (30)
S. Korea	70 (70)	10 (10)	70 (60)	10 (10)

Table 5-1: Premature mortalities using the EPA (WHO) CRF, rounded to nearest ten

Barrett et al. [10] uses the global-scale modeling results and the WHO CRF to estimate the aviation-attributable (normal fuel, full flight) health impacts of approximately 3500 premature mortalities from China and India combined. The regional-scale model used in this thesis work estimates approximately 4900 aviation-attributable premature mortalities; the global-scale model result is about 1.4 times smaller than the regional-scale model result, which is within multiplicative factor (factor of 1.4 to 2) computed for the U.S. region [11].

Also, for the countries listed in Table 5-1, the number of premature mortalities avoided due to the implementation of ULS fuel is compared to the global-scale equivalents from the

corresponding study [8]. Table 5-2 presents the comparison between the two modeling studies' results. The numbers outside the parentheses indicate the estimates using the EPA CRF, whereas the numbers inside the parentheses indicate the estimates using the WHO CRF.

	Full Flight		LTO Only	
	CMAQ	**GEOS-Chem**	**CMAQ**	**GEOS-Chem**
China	150 (80)	220 (72)	20 (10)	-150 (-13)
India	240 (260)	870 (390)	20 (10)	-55 (-15)
Bangladesh	30 (20)	80 (40)	0 (0)	0 (0)
Pakistan	20 (20)	100 (50)	0 (0)	-10 (0)
Japan	20 (30)	20 (10)	0 (20)	0 (0)
S. Korea	0 (10)	10 (0)	0 (0)	0 (0)

Table 5-2: Premature mortalities avoided due to ULS fuel implementation

When quantifying the number of mortalities avoided by implementing ULS fuel, the regional-scale model generally results in lower estimated $PM_{2.5}$ concentrations compared to the global-scale model results. The source of discrepancy between the results of different scale CTMs is not certain; thus, further investigations could be made to study how the aviation $PM_{2.5}$ concentrations vary spatially when downgrading from a global-scale model to a regional-scale model.

6 Conclusion

6.1 Summary

The Community Multiscale Air Quality (CMAQ) model was chosen and set up to establish a modeling platform that can simulate the air quality impacts of aviation emissions in Asia. In order to test the accuracy of this model setup and also to quantify biases, the CMAQ model was validated against measurements of ambient $PM_{2.5}$ concentration. This model, after validation, was setup to estimate the aviation air quality impacts on surface-level annual $PM_{2.5}$—the pollutant species highly correlated to adverse health impacts. For this modeling platform, the inputs to the CMAQ model were generated; these inputs include emission files (both background and aviation), boundary and initial conditions, meteorology, and others. Meteorological inputs were generated using a numerical weather prediction system called Weather Research and Forecasting (WRF) model; this modeling system was also validated against measurement data to ensure its validity.

With the proper model setup and emissions carefully put together, five one-year CMAQ simulations were performed: one background scenario and four aviation scenarios to study the air quality impacts and health impacts of various aviation scenarios. The results of these simulations showed that domain average of $15ng/m^3$ and $0.7ng/m^3$ increase in $PM_{2.5}$ concentrations were attributed to full flight and LTO-only aviation scenarios, respectively. The health impacts from the corresponding air quality impacts of aviation are computed; using the EPA (or WHO) CRF, the results estimate that approximately 9400 (6400) premature mortalities in Asia are attributed to both LTO and cruise cycles of aviation. Approximately 8000 (4900) of 9400 (6400) estimated premature mortalities are from China and India, the top two most populated countries in the world.

These results highlight a need for efforts by policymakers to mitigate the air quality impacts of aviation in Asia. More than 90% of the aviation-attributable premature mortalities are estimated to be associated with non-LTO (cruise) emissions; thus, in conjunction with a recent global-scale study [10], the results suggest that aircraft cruise emissions have significant health impacts in regional and global scales. Thus, in order to mitigate the adverse air quality and health impacts,

the effects of cruise emissions should also be considered. Also, implementation of ULS fuel in Asia is estimated to result in approximately 400 avoided premature mortalities in China and India combined. In addition to ULS fuel implementation, other approaches must be considered in efforts to mitigate the adverse air quality and health impacts of aviation in Asia.

6.2 Limitations & Future Work

One limitation of this thesis work is that there was a paucity of information needed to process the background emissions for the modeling domain. For example, the characteristics of power generation plant smokestacks were needed to accurately calculate the plume rise; however, due to the lack of information needed, an average value was used for all the power generation plants in Asia. Also, some of the temporal profiles and chemical speciation profiles were adapted from different regions of the world.

Another limitation of this work is that the secondary organics were not included in the air quality and health impacts analysis. Although the inorganic aerosols (sulfates, nitrates, and ammonium) take up a significant portion of the total $PM_{2.5}$ concentration, it is likely that the secondary organic aerosols will have a non-negligible part in perturbing the particulate matter concentration.

The Concentration-Response Functions (CRFs) used for premature mortality calculations can be another source of limitation for this thesis. As described in Chapter 5, the CRFs are obtained from epidemiological studies that took place primarily in the United States. Therefore, in order to apply the U.S.-based CRFs to the Asian domain, refinements must be made to ensure that the relationship between $PM_{2.5}$ concentration and premature mortalities is more suitable for the Asian domain.

As described in Section 3.2.5, the non-aviation emissions are generated using anthropogenic emissions of different sectors. Utilizing the sectorally separated emission files, a regional-scale air quality model—such as CMAQ—can be used to simulate the sector-specific air quality and health impacts. The sectors of the background emissions include power generation, industrial, road transportation, residential, and shipping; the one-year simulation results of various

emissions scenarios that exclude one sector at a time can be compared to the original background case the quantify the impacts of each emissions sector.

Bibliography

[1] Oxford Economics (2012). *Aviation Benefits Beyond Borders*. Air Transport Action Group: Geneva, Switzerland.

[2] The Boeing Company (2011). *Current Market Outlook: 2011-2030*. Boeing: Seattle, WA, U.S.

[3] Airbus (2011). *Global Market Forecast: 2011-2030*. Airbus: Blagnac Cedex, France.

[4] ICAO Secretariat (2010), *ICAO Environmental Report 2010: Aviation Outlook*. ICAO: Montréal, Québec, Canada.

[5] Rojo, J.J. (2007). *Future Trends in Local Air Quality Impacts of Aviation*. Master's Thesis, Massachusetts Institute of Technology.

[6] Mahashabd, A., Wolfe, P., Ashok, A., Dorbian, C. He, Q., Fan, A., Lukachko, S., Mozdzanowska, A., Wollersheim, C., Barrett, S. R. H., Locke, M., and Waitz, I. A. (2011). Assessing the environmental impacts of aircraft noise and emissions. *Progress in Aerospace Sciences*, Vol. 47, No. 1, Jan. 2011, pp. 15–52.

[7] Seinfeld, J. H. and Pandis, S. N. (2006). *Atmospheric Chemistry and Physics - From Air Pollution to Climate Change*, John Wiley & Sons., Hoboken, New Jersey, 2nd ed., 2006.

[8] Barrett, S. R., Yim, S. H., Gilmore, C. K., Murray, L. T., Tai, A. P., Kuhn, S. R., Yantosca, R. M., Byun, D., Ngan, F., Li, X., Ashok, A., Koo, J., Levy, J., Dessens, O., Balasubramanian, S., Fleming, G. G., Wollersheim, C., Malina, R., Pearlson, M. N., Stratton, R. W., Arunachalam, S., Binkowski, F. S., Jacob, D. J., Hileman, J. I., & Waitz, I. A. (2012). Public Health, Climate and Economic Impacts of Desulfurizing Aviation Fuel. *Environmental Science and Technology*.

[9] Barrett, S. R., Yim, S. H., Gilmore, C. K., Murray, L. T., Tai, A. P., Kuhn, S. R., Yantosca, R. M., Byun, D., Ngan, F., Li, X., Ashok, A., Koo, J., Levy, J., Dessens, O., Balasubramanian, S., Fleming, G. G., Wollersheim, C., Malina, R., Pearlson, M. N., Stratton, R. W., Arunachalam, S., Binkowski, F. S., Jacob, D. J., Hileman, J. I., & Waitz, I. A. (2012). Public Health, Climate and Economic Impacts of Desulfurizing Aviation Fuel (Supporting Information). *Environmental Science and Technology*.

[10] Barrett, S. R., Britter, R., & Waitz, I. A. (2010). Global mortality attributable to aircraft cruise emissions. *Environmental Science and Technology 44(19)*, 7736–7742.

[11] Barrett, S. R., Britter, R., & Waitz, I. A. (2010). Global mortality attributable to aircraft cruise emissions (Supporting Information). *Environmental Science and Technology 44(19)*, 7736–7742.

[12] Ratliff, G., Sequeira, C., Waitz, I., Ohsfeldt, M., Thrasher, T., Graham, M., & Thompson, T. (2009). *Aircraft Impacts on Local and Regional Air Quality in the United States*. Cambridge, MA: Partnership for AiR Transportation Noise and Emissions Reductions.

[13] Woody, M., Baek, B. H., Adelman, Z., Omary, M., Lam, Y. F., West, J. J., & Arunachalam, S. (2011). An assessment of Aviation's contribution to current and future fine particulate matter in the United States. *Atmospheric Environment 45(20)*, 3424-3433.

[14] Yim, S.H.L., Stettler, M.E.J., Barrett, S.R.H. (forthcoming) *Air Quality and Public Health Impacts of UK Airports—Part II: Impacts, Assessment and Policy Analysis*.

[15] United Nations, Department of Economic and Social Affairs, Population Division (2011). *World Population Prospects: The 2010 Revision, Highlights and Advance Tables*. ESA/P/WP.220.

[16] US EPA. (2007). *Guidance on the Use of Models and Other Analyses for Demonstrating Attainment of Air Quality Goals for Ozone, PM2.5, and Regional Haze*. Research Triangle Park, NC: US EPA OAQPS.

[17] Liu, X. (2010). Understanding of regional air pollution over China using CMAQ, part I: performance evaluation and seasonal variation, *Atmospheric Environment*, 44, 2415-2426.

[18] Zhang, Y. (2011). Application of MM5 in China: Model evaluation, seasonal variations, and sensitivity to horizontal grid resolutions, *Atmospheric Environment*, 45: 3454-3465

[19] Xing, J. (2011). Modeling study on the air quality impacts from emission reductions and atypical meteorological conditions during the 2008 Beijing Olympics, *Atmospheric Environment* 45: 1786-1798.

[20] Kwok, Roger H.F. (2010). Numerical study on seasonal variations of gaseous pollutants and particulate matters in Hong Kong and Pearl River Delta Region, *Journal of Geophysical Research*, 115, D16308.

[21] Wang, X. (2010). Process analysis and sensitivity study of regional ozone formation over the Pearl River Delta, China, during the PRIDE-PRD2004 campaign using the Community Multiscale Air Quality modeling system, *Atmospheric Chemistry and Physics*, 10, 4423-4437.

[22] CMAS. (2010). *Operational Guidance for the Community Multiscale Air Quality (CMAQ) Modeling System version 4.7.1 (June 2010 release)*. Chapel Hill, NC: Community Modeling and Analysis System, Institute for the Environment, University of North Carolina at Chapel Hill.

[23] Byun, D.W., Young, J., Pleim, J., Odman, M.T., and Alapaty, K. (1999). *Numerical Transport Algorithms for the Community Multiscale air Quality (CMAQ) Chemical Transport Model in Generalized Coordinates*. Research Triangle Park, NC: US EPA.

[24] Skamarock, W. C., J.B. Klemp, J. Dudhia, D. O. Gill, D.M. Barker, M.G. Duda, X. Huang, W. Wang, and J.G. Powers. (2008). A Description of the Advanced Research WRF Version 3, http://www.mmm.ucar.edu/wrf/users/docs/arw_v3.pdf

[25] Byun, D., Pleim, J.E., Tangm R.T., & Bourgeois, A. (1999). *Meteorology-Chemistry Interface Processor (MCIP) For Models-3 Community Multiscale Air Quality (CMAQ) Modeling System*. Research Triangle Park, NC: US EPA.

[26] U.S. National Centers for Environmental Prediction, updated daily: NCEP FNL Operational Model Global Tropospheric Analyses, continuing from July 1999. *Dataset ds083.2 published by the CISL Data Support Section at the National Center for Atmospheric Research, Boulder, CO, available online at* http://dss.ucar.edu/datasets/ds083.2/.

[27] CEMPD (2011). *SMOKE v2.7 User's Manual*, University of North Carolina at Chapel Hill. http://www.smoke-model.org/version2.7/SMOKE_v27_manual.pdf

[28] Wang, S., Zheng, J., Fu, F., Yin, S. and Zhong, L. (2011). Development of an emission processing system for the Pearl River Delta Regional air quality modeling using the SMOKE model: Methodology and evaluation. *Atmospheric Environment*, 45: 5079-5089

[29] Yarwood, G., Rao, S., Yocke, M., & Whitten, G. (2005). *Updates to the Carbon Bond Mechanism: CB05*. US EPA.

[30] Yantosca, B., Long, M., Payer, M., & Cooper, M. (2012) *GEOS-Chem v9-01-03 Online User's Guide*. Cambridge, MA, http://acmg.seas.harvard.edu/geos/doc/man/

[31] Lam, Y.F., and Fu, J.S. (2010). Corrigendum to "A novel downscaling technique for the linkage of global and regional air quality modeling" published in Atmos. Chem. Phys., 9, 9169-9185, 2009. *Atmospheric Chemistry and Physics* 10, 4013-4031.

[32] Willmott, C.J. (1981). On the validation of models. *Physical Geography,* 2, 184-194.

[33] NCDC (2012). *Global and U.S.—Integrated Surface Hourly*. Online Climate Data Directory, National Climatic Data Center. http://www.ncdc.noaa.gov/cdo-web/

[34] Appel, K.W., Gilliam, R.C., Davis N., Zubrow, A., & Howard, S.C. (2011). Overview of the atmospheric model evaluation tool (AMET) v1.1 for evaluating meteorological and air quality models. *Environmental Modeling and Software* 26(4), 434-443.

[35] Olivier, J.G.J. and J.J.M. Berdowski (2001) Global emissions sources and sinks. In: Berdowski, J., Guicherit, R. and B.J. Heij (eds.) "The Climate System", pp. 33-78. A.A.

Balkema Publishers/Swets & Zeitlinger Publishers, Lisse, The Netherlands. ISBN 90 5809 255 0.

[36] GEIA Center (2011). *Global Emissions Initiative (GEIA): Emission Reviews*, GEIA: Boulder, Colorado, USA.

[37] Akimoto, H. (2003). Global air quality and pollution, *Science*, 302, 1716-1719,

[38] Kato, N. and Akimoto, H. (1992). Anthropogenic emissions of SO_2 and NO_X in Asia: emissions inventories, *Atmospheric Environment*, 26, 2997-3017.

[39] Akimoto, H., and Narita, H. (1994). Distribution of SO_2, NO_X, and CO_2 emissions from fuel combustion and industrial activities in Asia with 1° × 1° resolution, *Atmospheric Environment*, 28, 213-225.

[40] Streets, D. G., et al. (2003), An inventory of gaseous and primary aerosol emissions in Asia in the year 2000, *Journal of Geophysical Research*, 108(D21), 8809, doi:10.1029/2002JD003093.

[41] Zhang, Q., D. G. Streets, G. R. Carmichael, K. B. He, H. Huo, A. Kannari, Z. Klimont, I. S. Park, S. Reddy, J. S. Fu, D. Chen, L. Duan, Y. Lei, L. T. Wang, and Z. L. Yao (2009), Asian emissions in 2006 for the NASA INTEX-B mission, *Atmospheric Chemistry and Physics, 9*, 5131-5153.

[42] Ohara, T., Akimoto, H., Kurokawa, J., Horii, N., Yamaji, K., Yan, X., and Hayasaka, T. (2007). An Asian emission inventory of anthropogenic emission sources for the period 1980-2020, *Atmospheric Chemistry and Physics*, 7, 4419-4444.

[43] A.H.W. Beusen, A.F. Bouwman, P.S.C. Heuberger, G. Van Drecht, and K.W. Van Der Hoek (2008). Bottom-up uncertainty estimates of global ammonia emissions from global agricultural production systems, *Atmospheric Environment*, Volume 42, Issue 24, August 2008, Pages 6067-6077, ISSN 1352-2310, DOI:10.1016/j.atmosenv.2008.03.044.

[44] Wang, C., J.J. Corbett, and J. Firestone (2007). Improving Spatial Representation of Global Ship Emissions Inventories, *Environmental Science & Technology*, Web Release Date: 01-Dec-2007;(Article) *DOI: 10.1021/es0700799*.

[45] Jacob, D.J., Crawford, J.H., Kleb, M.M., Connors, V.S., Bendura, R.J., Raper, J.L., Sachse, G.W., Gille, J.C., Emmons, L., and Heald, C.L. (2003). The Transport and Chemical Evolution over the Pacific (TRACE-P) aircraft mission: design, execution, and first results, *Journal of Geophysical Research*, 108, 9000, doi:10.1029/2002JD003276.

[46] IIASA (2001). RAINS-Asia CD-ROM Version 7.52, Laxenburg, Austria.

[47] Bouwman, A.F., et al. (1997). A global high-resolution emission inventory for ammonia. *Global Biogeochemical Cycles*, 11, 561-587.

[48] Endresen, Ø., E. Sørgård, J. K. Sundet, S. B. Dalsøren, I. S. A. Isaksen, T. F. Berglen, and G. Gravir (2003). Emission from international sea transportation and environmental impact, *Journal of Geophysical Research*, *108*, 4560, doi:10.1029/2002JD002898.

[49] Lauer, A., Eyring, V., Hendricks, J., Jöckel, P., and Lohmann, U. (2007). Global model simulations of the impact of ocean-going ships on aerosols, clouds, and the radiation budget, *Atmospheric Chemistry and Physics*, 7, 5061-5079, doi:10.5194/acp-7-5061-2007.

[50] Corbett, J.J., J.J. Winebrake, E.H. Green, P. Kasibhatla, V. Eyring, and A. Lauer (2007). Mortaility from Ship Emissions: A Global Assessment, *Environmental Science & Technology*, 41(24), 8512-8518, 2007.

[51] Hao, J., Wang, L., Shen, M., Li, L., and Hu. J. (2007). Air quality impacts of power plant emission in Beijing, *Environmental Pollution*, 147, 401-408.

[52] Wang X., Liang, X., Jiang, W., Tao, Z., Wang, J.X., Liu, H., Han, Z., Liu, S., Zhang, Y., Grell, G.A., and Peckham, S.E. (2010). WRF-Chem simulation of East Asian air quality: Sensitivity to temporal and vertical emissions distributions, *Atmospheric Environment*, 44, 660-669.

[53] Zhang, Q., Streets, D.G., HE, K., Wang, Y., Richter, A., Burrows, J.P., Uno, I., Jang, C.J., Chen, D., Yao, Z., and Lei, Y. (2007). NO_X emission trends for China, 1995-2004: The view from the ground and the view from space, *Journal of Geophysical Research*, 112, D22306, doi:10.1029/2007JD008684.

[54] Beijing Huatong Market Information Co. Ltd. (2006). China Latest Economic Indicators, Beijing.

[55] Wang, X., Jiang W., Liu, H., Wang, Y., and Zhang, Y. (2007). Numerical simulation study on the effect of major industrial sources in Nanjing on urban air quality. *Research of Environmental Science*, 20 (3), 33-43.

[56] WMO Global Atmosphere Watch. *World Data Centre for Greenhouse Gases*: http://ds.data.jma.go.jp/gmd/wdcgg/cgi-bin/wdcgg/catalogue.cgi, (accessed in 2012).

[57] Olivier, J., Peters, J., Granier, C., Pétron, G., Müller, J.F., & Wallens, S. (2003). Present and future surface emissions of atmospheric compounds. *POET Report #2*, EU project EVK2-1999-00011.

[58] Kannari, A., Tonooka, Y., Baba, T., & Murano, K. (2007). Development of multiple-species 1 km × 1 km resolution hourly basis emissions inventory for Japan. *Atmospheric Environment*, 41, 3428-3439.

[59] An, X., Zhu, T., Wang, Z., Li, C., & Wang, Y. (2007). A modeling analysis of a heavy air pollution episode occurred in Beijing, *Atmospheric Chemistry and Physics*, 7, 3103-3114.

[60] Koo, Y., Kim, S., Yun, H., Han, J., Lee, J., Kim, K., & Jeon, E. (2008). The simulation of aerosol transport over East Asia region, *Atmospheric Research*, 90, 264-271.

[61] Feng, Y., Wang, A., Wu, D., & Xu, X. (2007). The influence of tropical cyclone Melor on PM_{10} concentrations during an aerosol episode over the Pearl River Delta region of China: Numerical modeling versus observational analysis, *Atmospheric Environment*, 41, 4349-4365.

[62] Wei, X.L., Li, Y.S., Lam, K.S., Wang, A.Y. & Wang, T.J. (2007). Impact of biogenic VOC emissions on a tropical cyclone-related ozone episode in the Pearl River Delta region, China, *Atmospheric Environment*, 41, 7851-7864.

[63] Chen, D.S., Cheng, S.Y., Liu, L., Chen, T., & Guo, X.R. (2007). An integrated MM5-CMAQ modeling approach for assessing trans-boundary PM_{10} contribution to the host city of 2008 Olympic summer games—Beijing, China, *Atmospheric Environment*, 41, 1237-1250.

[64] Chen, X.L., Feng, Y., Li, J., Lin, W., Fan S., Wang, A., Fong, S., and Lin, H. (2009). Numerical Simulations on the Effect of Sea-Land Breezes on Atmospheric Haze over the Pearl River Delta Region, *Environmental Modeling and Assessment*, 41, 1237-1250.

[65] Bieser, J., Aulinger, A., Matthias, V., Quante, M., & Builtjes, P. (2011). SMOKE for Europe—adaptation, modification and evaluation of a comprehensive emission model for Europe, *Geoscientific Model Development*, 4, 47-68.

[66] Corbett, J.J. & Koehler, H.W. (2003). Updated emissions from ocean shipping, *Journal of Geophysical Research*, 108, 4650-4665.

[67] Levy et al. (2010). Health Impacts of Aviation-Related Air Pollutants, Project 11, PARTNER Advisory Board Meeting Presentation, NC.

[68] Ashok, A. (2011). *The Air Quality Impact of Aviation in Future-Year Emissions Scenarios*. Master's Thesis, Massachusetts Institute of Technology.

[69] Ratliff, G., Sequeira, C., Waitz, I., Ohsfeldt, M.,Thrasher, T., Graham, G., Thompson, T. (2009). *Aircraft Impacts on Local and Regional Air Quality in the United States*, Report No. PARTNER-COE-2009-002; PARTNER, 2009.

[70] Project for the Sustainable Development of Heathrow: Report of the Airport Air Quality Technical Panels (2006). U.K. Department for Transport.

[71] ICAO Air Transport Bureau. (2010). *Local Air Quality*. Retrieved July 16, 2011, from http://www.icao.int/icao/en/env2010/LocalAirQuality.htm

[72] Wayson, R., & Fleming, G. (2000). *Consideration of Air Quality Impacts by Airplane Operations at or above 3000 feet AGL*. Washington, D.C.: FAA Office of Environment and Energy.

[73] EDMS. (2010). *Emissions and Dispersion Modeling System (EDMS)*. Retrieved July 31, 2012, from http://www.faa.gov/about/office_org/headquarters_offices/apl/research/models/edms_model/

[74] Hileman, J. L., Stratton, R. W., & Donohoo, P.E. (2010). Energy content and alternative jet fuel viability. *Journal of Propulsion and Power*, 26 (6), 1184-1195.

[75] ASTM International, West Conshohocken, PA. (2007). *Standard Specification for Aviation Turbine Fuels, Std*. ASTM D1655-09, DOI: 10.1520/D1655-09.

[76] UK Ministry of Defence. (2011). *Defence Standard 91-91, Issue 7 (18 February 2011), Turbine Fuel, Kerosine Type, Jet A-1, NATO Code: F-35, Joint Service Designation: AVTUR*.

[77] Noel, G., Allaire, D., Jacobson, S., Willcox, K., & Cointin, R. (2009). Assessment of the Aviation Environmetnal Design Tool, *Eighth USA/Europe Air Traffic Management Research and Development Seminar (ATM2009)*.

[78] Baughcum, S. L., Tritz, T. G., Henderson, S. C., & Pickett, D. C. (1996). *Scheduled Civil Aircraft Emissions Inventories for 1992: Database Development and Analysis*. Hampton, VA: NASA Langley Research Center.

[79] Wayson, R. L., Fleming, G. G., & Iovinelli, R. (2009). Methodology to estimate particulate matter emissions from certified commercial aircraft engines. *Journal of Air and Waste Management 59*, 91-100.

[80] US EPA (2009). *Recommended Best Practice for Quantifying Speciated Organic Gas Emissions from Aircraft Equipped with Turbofan, Turbojet, and Turboprop Engines, version 1.0*. Washington D.C., USA.

[81] Stettler, M. E., Eastham, S., & Barrett, S. R. (2011). Air Quality and Public Health Impacts of UK Airports. Part I: Emissions. *Atmospheric Environment 45(31)* , 5415-5424.

[82] Binkowski, F. (1999). *The Aerosol Portion of Models-3 CMAQ*. Research Triangle Park, NC: US EPA.

[83] Cohen, A. J.; Anderson, H. R.; Ostro, B.; Pandey, K. D.; Krzyzanowski, M.; Kün̈zli, N.; Gutschmidt, K.; Pope, A.; Romieu, I.; Samet, J. M.; Smith, K. (2005). The global burden of disease due to outdoor air pollution *Journal of Toxicology and Environmental Health Part A*, 68 (13–14)1301– 1307

[84] Roman, H. A.; Walker, K. D.; Walsh, T. L.; Conner, L.; Richmond, H. M.; Hubbell, B. J.; Kinney, P. L. (2008). Expert judgment assessment of the mortality impact of changes in ambient fine particulate matter in the U.S *Environ. Sci. Technol.*, 42 (7) 2268– 2274

[85] Cooke, R. M.; Wilson, A. M.; Tuomisto, J. T.; Morales, O.; Tainio, M.; Evans, J. S. A probabilistic characterization of the relationship between fine particulate matter and mortality: Elicitation of European experts *Environ. Sci. Technol.* 2007, 41) 6598– 6605

[86] Pope III, C. A. (2007). Mortality effects of longer term exposures to fine particulate air pollution: Review of recent epidemiological evidence *Inhalation Toxicol.*, 19, 33– 38

[87] Cohen, A. J.; Anderson, H. R.; Ostro, B.; Pandey, K. D.; Krzyzanowski, M.; Kuenzli, N.;Gutschmidt, K.; Pope, C. A.; Romieu, I.; Samet, J. M.; Smith, K. R. (2004). Mortality impacts of urban air pollution. In *Comparative Quantification of Health Risks: Global and Regional Burden of Disease Due to Selected Major Risk Factors*; Ezzati, M.; Lopez, A. D.; Rodgers,A.; Murray, C. U. J. L., Eds.; World Health Organization: Geneva, 2004; Vol. 2.

[88] Pope III, C. A.; Burnett, R. T.; Thun, M. J.; Calle, E. E.; Krewski, D.; Ito, K.; Thurston, G. D. (2002). Lung cancer, cardiopulmonary mortality, and long-term exposure to fine particulate air pollution *J. Am. Med. Assoc.* 2002, 287 (9) 1132– 1141

[89] Ostro, B. (2004) *Outdoor Air Pollution: Assessing the Environmental Burden of Disease at National and Local Levels. Environmental Burden of Disease Series, No. 5*; World Health Organization: Geneva.

[90] US Environmental Protection Agency. (2011). *The Benefits and Costs of the Clean Air Act: 1990 to 2020*. Washington, DC: Office of Air and Radiation.

[91] Cohen, A.J. (2003). Air Pollution and Lung Cancer: What More Do We Need to Know? *Thorax*. 58, 1010-1012.

[92] Center for International Earth Science Information Network (CIESIN), Columbia University; United Nations Food and Agriculture Programme (FAO); and Centro Internacional de Agricultura Tropical (CIAT). (2005). Gridded Population of the World: Future Estimates (GPWFE). Palisades, NY: Socioeconomic Data and Applications Center (SEDAC), Columbia University. Available at http://sedac.ciesin.columbia.edu/gpw.

[93] World Health Organization. *Global Burden of Disease (GBD);* http://www.who.int/healthinfo/global_burden_disease/en/.

[94] Hong Kong Environmental Protection Department: *Past Air Quality Monitoring Data*: http://epic.epd.gov.hk/ca/uid/airdata/p/1, (accessed in 2011).

[95] Taiwan Air Quality Monitoring Network. *History Data Download*: http://taqm.epa.gov.tw/taqm/en/YearlyDataDownload.aspx, (accessed in 2011).

Appendix A: CMAQ Model Build Parameters

Module	Option
Mechanism	cb05cl_ae5_aq
ModAdepv	module aero_depv2
ModAdjc	module
ModAero	module aero5
ModChem	module ebi_cb05cl_ae5
ModCloud	module cloud_acm_ae5
ModCpl	module gencoor
ModDriver	module ctm_yamo
ModHadv	module hyamo
ModHdiff	module multiscale
ModInit	module init_yamo
ModPa	module pa
ModPhot	module phot_table
ModUtil	module util
ModVadv	module vyamo
ModVdiff	module acm2
PAOpt	pa_noop
Tracer	trac0

Appendix B: List of Emission Species

ALD2
ALDX
CO
ETH
ETHA
ETOH
FORM
HONO
IOLE
MEOH
NH3
NO
NO2
NR
OLE
PAR
PEC
PMC
PMFINE
PNO3
POA
PSO4
SO2
SO4
TOL
UNR
XYL

Appendix C: NMVOC Speciation for Background Emissions

NMVOC split factors for each emission sector for CB05 lumped species

CB05 lumped Species	Industry	Power Generation	Residential	Road Transport	Shipping
PAR	0.03150	0.01366	0.03416	0.04479	0.04908
OLE	0.00029	0.00025	0.00061	0.00120	0.00100
TOL	0.00049	0.00051	0.00024	0.00087	0.00045
XYL	0.00028	0.00122	0.00005	0.00080	0.00041
FORM	0.00705	0.01833	0.00075	0.00162	0.00210
ALD2	0.00000	0.00000	0.00000	0.00043	0.00056
ETH	0.00149	0.00030	0.00466	0.00239	0.00262
ETOH	0.00046	0.00000	0.00250	0.00000	0.00000
NR	0.01161	0.00206	0.01094	0.00291	0.00526
ETHA	0.00128	0.00118	0.00255	0.00051	0.00015
UNR	0.00055	0.00071	0.00369	0.00394	0.00694

Appendix D: NMVOC Speciation for Aviation Emissions

CB05 lumped Species	Split Factors
PAR	0.0265337999978819
OLE	0.0028573572615178
TOL	0.0002305105270003
XYL	0.0002220045004653
FORM	0.0047059286925961
ALD2	0.0009960348982553
ETH	0.0055106041614521
MEOH	0.0005633255996999
ETHA	0.0001734177270832
IOLE	0.0004093060432251
ALDX	0.0015602739008786
UNR	0.0033673830947365